

CZECH TECHNICAL UNIVERSITY IN PRAGUE

Faculty of Electrical Engineering

Department of Electromagnetic Field



## MASTER THESIS

**Polarization diversity antenna**

Anténa s polarizační diverzitou

**May 2016**

**Master student: Bc. Gábor Korpás**  
**Thesis supervisor: doc. Ing. Pavel Hazdra, Ph.D.**

České vysoké učení technické v Praze  
Fakulta elektrotechnická

katedra elektromagnetického pole

## ZADÁNÍ DIPLOMOVÉ PRÁCE

Student: **Bc. Gábor Korpás**

Studijní program: Komunikace, multimédia a elektronika

Obor: Bezdrátové komunikace

Název tématu: **Anténa s polarizační diverzitou**

Pokyny pro vypracování:

Navrhněte planární anténu s polarizační diverzitou, které bude dosaženo buzením různých modů na zářiči obdélníkového tvaru. Pro návrh užití analyzátoru charakteristických modů v MATLABu (příslušné kódy jsou dostupné na katedře), zaměřte se na možnosti vybuzení dvou navzájem kolmých modů kapacitní a induktivní vazbou. Stanovte vliv rozměrů vazebních elementů na vstupní impedanci, tvary proudových distribucí a vyzářovací diagram. Pro Vámi vybraný typ vazebního členu proveďte simulaci kompletní struktury v CST MWS včetně řešení přizpůsobení k 50 Ohm koaxiálnímu kabelu. Vzorek antény vyrobte a vlastnosti ověřte měřením. Frekvenční pásmo bude upřesněno v průběhu řešení s ohledem na výrobní možnosti a hodnoty diskretních prvků přizpůsobovacího obvodu.

Seznam odborné literatury:

- [1] Martens, R., Safin, E., Manteuffel, D., "Selective excitation of characteristic modes on small terminals", EuCAP 2011
- [2] Martens, R., Safin, E., Manteuffel, D., "Inductive and capacitive excitation of the characteristic modes on small terminals", LAPC 2011
- [3] Araghi, A., Dadashzadeh, "Oriented design of an antenna for MIMO applications using theory of characteristic modes", IEEE AWPL, vol. 11, 2012

Vedoucí: doc. Ing. Pavel Hazdra, Ph.D.

Platnost zadání: LS 2016/2017



prof. Ing. Pavel Pechač, Ph.D.  
vedoucí katedry

prof. Ing. Pavel Ripka, CSc.  
děkan

V Praze dne 27. 1. 2016

## Čestné prohlášení

Prohlašuji, že jsem zadanou diplomovou práci zpracoval sám s přispěním vedoucího práce a konzultanta a používal jsem pouze literaturu v práci uvedenou. Dále prohlašuji, že nemám námitek proti půjčování nebo zveřejňování mé diplomové práce nebo její části se souhlasem katedry.

Datum: 27. 5. 2016

.....  
podpis diplomanta

## Poděkování

Chtěl bych poděkovat panu doc. Ing. Pavlovi Hazdrovi, Ph.D. za odborné vedení práce a cenné rady, které mi pomohly tuto práci zkompletovat. Mé poděkování patří též celé Katedře elektromagnetického pole za spolupráci při realizování navrhnuté antény a získávání údajů pro praktickou část práce.

## Abstrakt:

Tato diplomová práce se zabývá problematikou antén s polarizační diverzitou, která je dosažena selektivním buzením různých modů na zářiči. Takové antény lze efektivně používat v MIMO systémech. Buzení jednotlivých modů je vyšetřeno pomocí teorie charakteristických modů (TCM). Práce se skládá ze dvou částí. První část se zaměřuje na vybudění těchto modů pomocí induktivních a kapacitních vazebních členů. Je provedena rešerše a porovnání existujících řešení. Dále je namodelována konkrétní anténa v simulačním prostředí MATLAB a v software CST. V druhé části práce módy jsou vybudeny pomocí zářiče ve tvaru L. Je navrhována a simulována patch anténa v programu CST. Dále, tato anténa je vyrobena a změřena pro ověření simulačních výsledků v praxi.

**Klíčová slova:** polarizační diverzita, teorie charakteristických modů (TCM), multiple-input and multiple-output (MIMO) systémy, selektivní buzení, vazební členy, L-probe (zářič ve tvaru L)

## Abstract:

This master thesis deals with the problematics of polarization diversity antennas. This polarization diversity is achieved by selective excitation of different modes on the radiation element. These antennas are very useful in MIMO systems. The excitation of selected modes is based on the TCM (Theory of Characteristic Modes). This paper consists of two parts. The first part focuses on excitation of these modes by inductive and capacitive coupling elements. The existing solutions are summarized and compared. To show the correctness of these methods, a concrete antenna is designed and simulated in MATLAB and in CST software. In the second part the excitation is achieved by a radiator in shape of L. A patch antenna is designed and simulated in CST. Furthermore, this antenna is constructed and measured to verify the results of the simulation in practice.

**Index Terms:** polarization diversity, Theory of Characteristic Modes (TCM), multiple-input and multiple-output (MIMO) systems, selective excitation, coupling elements, L-probe, reconfigurable antennas

# Table of contents

List of Tables.....	viii
List of Figures .....	ix
List of symbols and abbreviations.....	xi
Chapter 1.....	1
Introduction .....	1
Chapter 2.....	3
Theory of Characteristic Modes (TCM) .....	3
2.1 Introduction to the TCM .....	3
2.2 Definition of TCM .....	3
2.3 Modal superposition .....	4
2.4 Eigenvalues and characteristic angles.....	4
Chapter 3.....	6
Polarization diversity antennas.....	6
3.1 Multiple-Input and Multiple-Output.....	6
3.2 MIMO Channel .....	6
3.3 A different point of view on MIMO.....	7
3.4 The polarization diversity of antennas.....	7
Chapter 4.....	8
The inductive and capacitive coupling elements .....	8
4.1 Existing solutions.....	8
4.2 Inductive coupling elements .....	9
4.3 Capacitive coupling elements .....	10
4.4 Excitation by coupling elements .....	10
4.5 Excitation by ICE.....	12
4.6 Excitation by CCE.....	14
4.7 Radiation patterns.....	16
4.8 Radiation pattern cross cut .....	20
4.9 Impedance matching.....	20
4.10 Summary of the coupling elements .....	21
Chapter 5.....	22
L-probe feeding system.....	22
5.1 Introduction .....	22
5.2 L-probe systems .....	22

5.3	Equivalent circuit.....	23
5.4	The design process.....	23
5.5	Parameter sweep simulations.....	24
5.6	The designed antenna.....	25
5.7	Properties of the designed antenna .....	26
5.8	Envelope cross correlation.....	30
5.9	Characteristic modes of the designed antenna .....	31
5.10	The fabricated sample.....	34
5.11	Summary of the L-probe feeding system.....	37
Chapter 6.....		38
Conclusion.....		38
References.....		40
Appendix.....		43

# List of Tables

Table 1: List of important symbols.....	xi
Table 2: List of abbreviations .....	xi
Table 4.1: The comparison of the 3D radiation pattern diagrams for ICE model.....	17
Table 4.2: The comparison of 3D radiation pattern diagrams for CCE model .....	19
Table 4.3: The comparison of cross cut radiation pattern diagrams in CST software .....	19
Table 4.4: ICE – impedance matching circuits.....	20
Table 4.5: CCE – impedance matching circuits .....	21
Table 5.1: The parameters of the designed antenna .....	25
Table 5.2: 3D radiation patterns of the designed antenna .....	28
Table 5.3: Polar cut radiation diagrams of the designed antenna.....	29
Table 5.4: The surface current distribution for first six modes of the designed antenna	33
Table 5.5: Far-field radiation patterns of Mode 3 and 6 of the designed antenna .....	33
Table 5.6: The dimension changes for the fabricated antenna .....	34
Table 5.7: Comparison of the polar cut radiation patterns from the simulation and measurement.....	36



# List of Figures

Figure 3.1: Example of 4x4 MIMO system .....	6
Figure 4.1: Current distribution at the edge of the patch for first three modes (a), optimal position for inductive (b) and for capacitive coupling elements (c) [22].....	8
Figure 4.2: Symmetrical wire loop (left) and the non-symmetrical integrated coupling element at the edge of the patch (right) .....	9
Figure 4.3: Non-resonating coplanar capacitive coupling element in the corner of the patch .....	10
Figure 4.4: The generated mesh of the original patch.....	11
Figure 4.5: Characteristic angles, original patch .....	11
Figure 4.6: Eigenvalues of the modes, original patch .....	11
Figure 4.7: Original patch – mode $J_1$ .....	12
Figure 4.8: Original patch – mode $J_2$ .....	12
Figure 4.9: The generated mesh, ICE .....	12
Figure 4.10: The dimensions of the coupling slots.....	13
Figure 4.11: Characteristic angles, ICE .....	13
Figure 4.12: Eigenvalues, ICE .....	13
Figure 4.13: ICE – mode $J_1$ .....	14
Figure 4.14: ICE – mode $J_2$ .....	14
Figure 4.15: The dimensions of the capacitive coupling elements.....	14
Figure 4.16: The generated mesh, CCE .....	15
Figure 4.17: Characteristic angles, CCE .....	15
Figure 4.18: Eigenvalues, CCE .....	15
Figure 4.19: CCE – mode $J_1$ .....	16
Figure 4.20: CCE – mode $J_2$ .....	16
Figure 4.21: The ICE model in CST with the connected discrete ports .....	16
Figure 4.22: The CCE model with connected discrete ports .....	18
Figure 5.1: The principle of the L-probe system .....	22
Figure 5.2: Parasitic components.....	23
Figure 5.3: The parameters and the layout of the designed antenna (dimensions in mm) .....	26
Figure 5.4: The designed antenna model in CST.....	26
Figure 5.5: The return loss parameter ( $S_{11}$ and $S_{22}$ ) of the designed antenna .....	27
Figure 5.6: The isolation ( $S_{12}$ and $S_{21}$ ) between the ports.....	27
Figure 5.7: The difference between polarizations .....	29
Figure 5.8: Envelope cross correlation computed with two methods.....	30
Figure 5.9: Characteristic angles of the designed antenna – patch only .....	31
Figure 5.10: The first three characteristic modes of the patch .....	31

Figure 5.11: The characteristic mode analysis of the ground plane itself .....	32
Figure 5.12: The characteristic mode analysis of the ground plane and the L-probes.....	32
Figure 5.13: Characteristic angles of the complete designed antenna.....	33
Figure 5.14: Production of the antenna sample .....	34
Figure 5.15: The fabricated antenna in the anechoic chamber .....	35
Figure 5.16: The return loss of the fabricated antenna .....	35
Figure 5.17: The polarization of the fabricated antenna .....	37
Ap. 1: Parameter sweep simulation, H = 24-32 mm, W = 85-105 mm, L <sub>v</sub> = 20 mm, L <sub>h</sub> = 32 mm .....	43
Ap. 2: Parameter sweep simulation, H = 24-32 mm, W = 95 mm, L <sub>v</sub> = 20 mm, L <sub>h</sub> = 26-38 mm .....	44
Ap. 3: Parameter sweep simulation, H = 26 mm, W = 95 mm, L <sub>v</sub> = 18-22 mm, L <sub>h</sub> = 26-34 mm .....	45

# List of symbols and abbreviations

$\lambda_n$	Eigenvalue of a characteristic mode
$J_n$	Characteristic current
$\mathbf{Z} = \mathbf{R} + j\mathbf{X}$	Complex matrix of mutual impedances
$E_n$	Characteristic electrical field
$J$	Surface current density
$V_n$	Modal excitation coefficient
$\alpha_n$	Characteristic angle
$\lambda$	Wavelength
$f_c$	Resonance frequency
$c$	Speed of the light
$L$	Length of the patch
$W$	Width of the patch
$H$	Height of the patch
$L_v$	Length of the vertical part of the L-probe
$L_h$	Length of the horizontal part of the L-probe
$D$	Difference between the position of the vertical part of the L-probe and the patch edge
$\rho$	Envelope cross correlation
$\Omega$	Full solid angle
$\Delta$	Difference

Table 1: List of important symbols

TCM	Theory of Characteristic Modes
MIMO	Multiple-Input and Multiple-Output
SISO	Single-Input and Single-Output
SIMO	Single-Input and Multiple-Output
MISO	Multiple-Input and Single-Output
ICE	Inductive coupling element
CCE	Capacitive coupling element

Table 2: List of abbreviations

## Chapter 1

# Introduction

In the last decades, the wireless technology went through an enormous development. It has spread to the everyday use; nowadays number of devices capable of wireless connectivity can be found in almost every household. People like to use their smartphones, tablets and laptops in every place and situation: at home, in the office, using the public transport, etc. They want their device to connect to the home Wi-Fi network and in the meantime they want to make calls over the mobile network. This means, that these handheld devices should operate simultaneously in different frequency bands and use different technologies. This is a big challenge for the manufacturers. They need to design their products in a way, so that it can be effectively used in every part of the world: in places, where the old GSM standard is still in use or in other places, where is possible to watch online videos in HD quality through the packet-oriented LTE network. This requires the antenna of the device to be able to meet the criteria and cover all frequency bands. The design of that complex antenna is not an easy task: it should be lightweight, small, compact, thin, robust and flexible at the same time. [1]

Unfortunately, if the shape of the antenna is too complicated, it is hard to find design rules and equations, which let us control the direction of the development. In these cases, numerical methods [2,3] and electromagnetic simulators, such as IE3D, FEKO, Empire and HFSS can be used. With the help of these simulators, the properties of the designed antenna can be examined before it goes into production. The availability of powerful computers makes this process a lot easier, but the final structure still strongly depends on the experience of the designer. It is often required to optimize the modeled antenna in experimental way.

Another possibility to develop an antenna is the usage of automatic optimization methods. These methods are based on pseudo-random search algorithms [4]. The biggest advantage is that the final product is sufficiently satisfactory, only a minimal refining needs to be done by the designer, the hardest part of the work is made by computer.

The above mentioned methods are mostly suitable for antenna design, but they have one significant disadvantage: they don't respect the real knowledge and principles, they don't have the physical insight about how antennas operate. There exists a not well known, but in recent years more and more used method, which efficiently solves this problem: it is called the Theory of Characteristic Modes (TCM).

In this master thesis TCM will be used to analyze the modes of different patch antennas. The goal is to achieve polarization diversity by exciting two degenerative modes on the patch. This can be achieved by different excitation elements as it will be showed later. The structure of this work is the following. First, the basic theory of TCM method will be discussed. Then, the whole thesis can be divided into two parts.

In the first part, the excitation of required modes is done by coupling elements, such as inductive and capacitive coupling elements. In this part, the existing solutions will be revived and summarized. To test these solutions in practice, a square patch antenna is designed and simulated both in MATLAB simulation environment [5] and CST Design Studio [6]. The radiation pattern will be compared in both cases. Afterwards, an impedance matching circuit will be suggested for each scenario.

In the second part, a radiator in the shape of letter L, so called L-probe will be used as the exciter. The modeling process is described in detail. It is showed how different parameters affect the properties, such as the S-parameters of the antenna. For this purpose, the antenna is modeled in CST software. After choosing the best parameters for the proposed antenna, characteristic mode analysis is calculated. The final design is also manufactured and measured in the anechoic chamber. The results of the simulation and measurement will be compared and discussed in the end.

## Chapter 2

# Theory of Characteristic Modes (TCM)

### 2.1 Introduction to the TCM

The Theory of Characteristic Modes was first published and described by Garbacz [7] at the end of the sixties of the 20<sup>th</sup> century. A few years later it was refined by Harrington and Mautz [8], [9]. The biggest advantage of this theory is that modal solutions can be formulated not only for very complex and arbitrary conducting bodies, but for apertures and another structures, which are capable of showing any kind of resonance. This can be very helpful in solving problems related to analysis, synthesis and optimization of antenna structures [10-12]. Unfortunately, with the development of sophisticated simulators of electromagnetic field, the TCM was somewhat forgotten.

### 2.2 Definition of TCM

According to the definition, characteristic modes are individual currents obtained numerically for any kind of conducting bodies with arbitrary shapes [7]. By the fact, that these modes provide quite accurate information about possible radiation patterns, are these modes very important for the design of the antenna. The characteristic modes are independent from the excitation, they are dependent only on the shape and the size of the conductive object. Because of this, the antenna design can be divided into two parts. The first part is the optimization of the shape and the size of the radiating element. This way the required resonant central frequency and radiation properties can be adjusted. If the size of the element is either minimized or enlarged, the resonant frequency will be also changed. The same is the situation with radiation properties. After that, in the second part, it is necessary to find the appropriate feeding configuration which excites the selected modes [13]. This can be done for example with coupling elements or with L-probes, as will be showed later in this work. For a correct antenna design, usually a few dominant modes are sufficient to be analyzed.

According to [8], characteristic modes or characteristic currents can be derived by the eigenfunctions of the following particular eigenvalue equation:

$$X\mathbf{J}_n = \lambda_n R\mathbf{J}_n, \quad (1)$$

where

- $\lambda_n$  is the eigenvalue
- $\mathbf{J}_n$  is the  $n$ -th eigenvector or the characteristic current
- $R$  and  $X$  are the real and imaginary part of the generalized impedance operator  $Z$ .

The impedance operator is formed as:

$$Z = R + jX. \quad (2)$$

This impedance operator can be obtained after forming an integro-differential equation. Because of the reciprocity theorem, if  $Z$  is a linear symmetric operator, its Hermitian parts  $R$  and  $X$ , will be a real and a symmetric operator as well. This means, that all eigenvalues  $\lambda_n$  in the Eq. (1) are real and all the eigenvectors  $\mathbf{J}_n$  can be chosen real or equiphase over the surface on which they are defined. Moreover, the choice of  $R$  as weight operator is

responsible for the orthogonality properties of characteristic modes. More information can be found in [8].

In practice, it is more effective to use the impedance operator in matrix form with the help of Galerkin formulation [14]:

$$\mathbf{X}\mathbf{J}_n = \lambda_n \mathbf{R}\mathbf{J}_n. \quad (3)$$

After this, the eigenvectors of characteristic currents  $\mathbf{J}_n$  and the eigenvalues  $\lambda_n$  can be computed solving the Eq. (3) with standard algorithms.

## 2.3 Modal superposition

Characteristic currents  $\mathbf{J}_n$  on the surface of a conductive body are producing electrical fields  $\mathbf{E}_n$ , which are called characteristic fields. These characteristic fields, such as the characteristic currents, are orthogonal to each other. As a consequence, characteristic modes are radiating independently from each other. The total current  $\mathbf{J}$  on the surface of the conductive body can be obtained as modal superposition of individual characteristic currents  $\mathbf{J}_n$ . The derivation of the following equation can be found also in [6].

$$\mathbf{J} = \sum_n \alpha_n \mathbf{J}_n = \sum_n \frac{V_n^i \mathbf{J}_n}{1 + j\lambda_n} \quad (4)$$

In the Eq. (4)

- $\alpha_n$  denotes the weighting coefficient and
- $V_n^i$  denotes the modal excitation coefficient. This coefficient represents how the  $n$ -th characteristic current mode influences the entire current distribution.

## 2.4 Eigenvalues and characteristic angles

In the Eq. (4), the expression  $\lambda_n$  corresponds to the eigenvalue associated with the  $n$ -th characteristic mode. This eigenvalue is very important due to the fact that its magnitude gives information about how well the particular mode radiates. The mode, which has its eigenvalue zero,  $|\lambda_n = 0|$ , is resonating. This means, the smaller the magnitude of the eigenvalue, the more efficiently the excited mode radiates. Moreover, the sign of the eigenvalue defines whether the particular mode contributes to electric ( $\lambda_n < 0$ ) or magnetic energy ( $\lambda_n > 0$ ) storing.

There is also another way to express the eigenvalues and that is to use characteristic angles  $\alpha_n$ . Characteristic angles are defined according to [15] as follows:

$$\alpha_n = 180^\circ - \tan^{-1}(\lambda_n). \quad (5)$$

The advantage of characteristic angles is that their value changes more rapidly so they are better for analysis. From physical point of view these angles return the phase difference between characteristic currents  $\mathbf{J}_n$  and the associated characteristic field  $\mathbf{E}_n$ . A certain mode resonates if  $\lambda_n = 0$  which in characteristic angle scale means  $\alpha_n = 180^\circ$ . So if the characteristic angle is close to  $180^\circ$ , the excited mode radiates efficiently. In cases when  $\alpha_n$  is close to  $90^\circ$  or  $270^\circ$ , the mode mainly stores energy. The situation with eigenvalues  $\lambda_n$  and characteristic angles  $\alpha_n$  can be summarized as follows:

- $\lambda_n = 0$  ( $\alpha_n = 180^\circ$ )  $\rightarrow$  mode is resonating,

- $\lambda_n < 0$  ( $\alpha_n > 180^\circ$ )  $\rightarrow$  mode has a capacitive character,
- $\lambda_n > 0$  ( $\alpha_n < 180^\circ$ )  $\rightarrow$  mode has an inductive character.

Furthermore, the frequencies related to angles between  $135^\circ$  and  $225^\circ$  represent the radiating bandwidth of the excited mode.

In this thesis characteristic mode analysis will be executed using the software CST Design Studio and a MATLAB tool developed by the Department of Electromagnetic Field in Czech Technical University in Prague within a diploma thesis [16].



# Polarization diversity antennas

## 3.1 Multiple-Input and Multiple-Output

The 4<sup>th</sup> generation wireless communication systems are capable of transmitting data with high speed. To satisfy these increased demands on capacity and throughput of the mobile device, the technology called Multiple-Input and Multiple-Output (MIMO) can be used. MIMO systems are also a good solution for wearable sensors, because these systems are resistant against transmission losses caused by the presence of the human body [17].

Originally, MIMO systems used different antennas or antenna arrays for signal transmission and reception. These antennas were separated by half of the wavelength or more from each other. For such purposes a PIFA (Planar Inverted F-Antenna) antenna, for instance, can be used.

The MIMO technology constitutes the major breakthrough in wireless communication system by increasing the channel capacity without increasing the transmitted power of antenna, which leads to green wireless network. MIMO technology provides benefits over a simple transmission technology, such as array gain, spatial diversity gain, spatial multiplexing gain and interference reduction. One possible MIMO solution is represented in Fig. 3.1. [18].

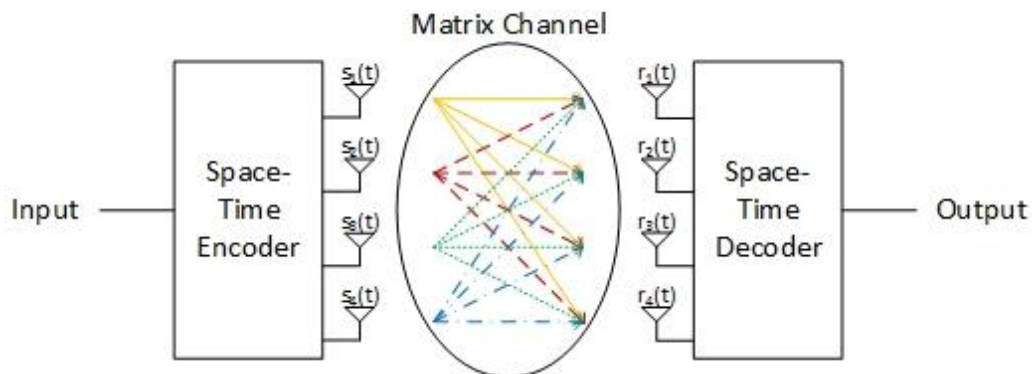


Figure 3.1: Example of 4x4 MIMO system

## 3.2 MIMO Channel

According to [19], various solutions of MIMO method can be used depending on the situation:

- SISO (Single-Input and Single-Output) – this technique refers to a classic way of transmission, where only a single antenna is used on the transmitter and the receiver side. This technic is more sensitive to interference and fading.
- SIMO (Single-Input and Multiple-Output) – it is a simplified version of MIMO, where the transmitter side has only one antenna, but the receiving place is equipped with multiple antenna units. This technic can be an efficient way to fight the negative effect of transmission fading.

- MISO (Multiple-Input and Single-Output) – This method is the opposite of SIMO.
- MIMO – Using this technology better communication coverage and transmission quality is achieved. The MIMO channel system can be described by the number of antenna elements on the transmitter and receiver side. There are solutions using 2x2, 4x4, 8x8 and even 12x12 antennas.

### 3.3 A different point of view on MIMO

The integration of MIMO antenna systems to a mobile device is not an easy task, with regard to the fact that these mobile devices are very limited in size. Moreover, it is necessary to use good isolation and sufficient separation between antenna elements, if high performance wants to be achieved.

However, a more attractive solution that enables compact MIMO system design, is the use of various modes for radiation. This can be achieved by exciting different characteristic modes on the small antenna terminal. Thanks to this, using only one antenna element, independent radiation patterns can be achieved. The properties of these radiation patterns are comparable with MIMO systems formed from multiple antennas or antenna arrays [20].

### 3.4 The polarization diversity of antennas

It was proven, that the most effective antenna of a mobile device is the chassis, resp. the PCB (Printed-Circuit-Board) of the device itself. Theory of Characteristic Modes describes the distribution of currents on conductive surface – the chassis of the mobile device, for example – like superposition of several mutually orthogonal characteristic modes. These modes can be efficiently excited with non-resonating coupling elements. The bandwidth of small terminal antennas can be optimized by exciting several modes by a common coupling element [13].

According to the fact that these modes are orthogonal, this principle can be used for the design of MIMO systems. For this, it is important to know the distribution of surface currents on the structure and the behavior of the characteristic modes. For these purposes characteristic mode analysis can be used. Further, it is necessary to calculate how the different modes contribute to the radiation of the entire structure. The most important part of the design is finding the appropriate coupling element for selective excitation of the required modes.

## Chapter 4

# The inductive and capacitive coupling elements

### 4.1 Existing solutions

In this master thesis existing solutions are investigated for exciting required modes. In the examined works the frequently used excitation techniques are by inductive or by capacitive coupling elements.

In [21] a rectangular conductive plate with width  $a = 60 \text{ mm} = \lambda/2$  and length  $b = 120 \text{ mm} = \lambda$  is examined, where  $\lambda$  refers to the wavelength. The choice of these dimensions is quite reasonable, because modern mobile phones have approximately the same size. As it was mentioned before, the shape and the dimensions of the antenna terminal have an effect on the resonance frequency. Therefore, in this case, the resonance frequency will be around  $f_c = 2.5 \text{ GHz}$ .

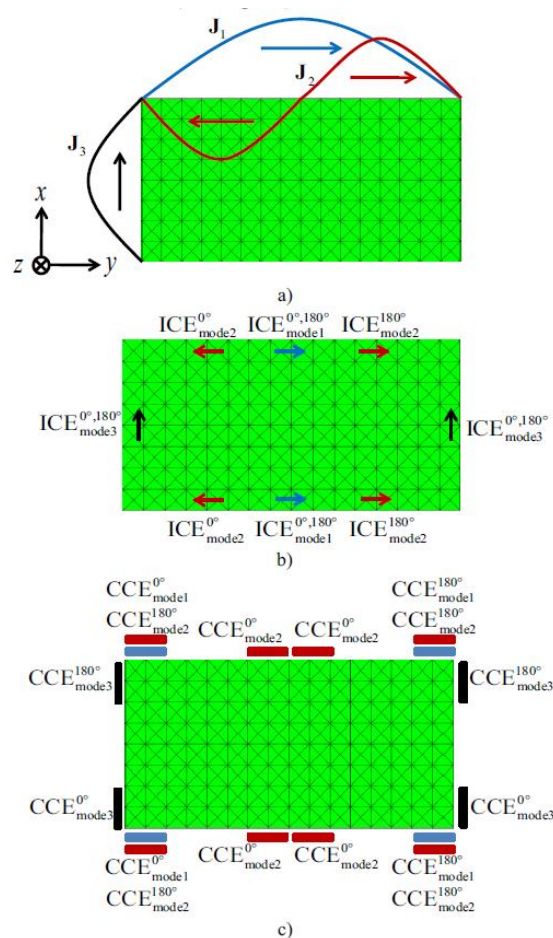


Figure 4.1: Current distribution at the edge of the patch for first three modes (a), optimal position for inductive (b) and for capacitive coupling elements (c) [22]

The dominant modes can be selectively excited with canonical concentrated exciters on the rectangular plate. The specific current distributions can be characterized

with sinusoidal behavior alongside the edges of the plate. Figure 4.1a shows the position of excited dominant modes  $J_1$ ,  $J_2$  and  $J_3$ . Eigenvalues of this modes are close to zero for resonance frequency. Modes  $J_1$  and  $J_2$  are half wavelength resonance modes along the major and minor axes, mode  $J_3$  is a one wavelength resonance mode along the major axes. The radiation patterns, which can be found in [21], are orthogonal.

The current distributions have their maxima and minima at certain places. In addition to the current distribution the voltage distribution, resp. distribution of electric field can be investigated on the plate. The electrical field and the current distribution have a 90-degree phase difference. This means, that the voltage distribution will have its minima in places, where current distribution has their maxima and vice versa. Because of this reason, a particular mode can be excited by inductive coupling element (ICE) placed to the location, where current distribution is at the maximum. Capacitive coupling elements (CCE) should be placed to the locations, where current distribution has its minima. This principle is depicted on the Fig. 4.1b and 4.1c.

## 4.2 Inductive coupling elements

Ideally, the coupling element is able to excite the current distribution of required mode without strongly influencing the radiation properties of the whole antenna element. In practice, ICE can be realized as follows. It can be imagined as a non-resonating narrow wire loop. Let's assume a source in one arm of the loop, which excites a current flow. If the wire loop is electrically small, the same current will flow in the other arm of the loop. Because of the arms of the loop are in close vicinity, the electrical fields generated by them cancel each other. The length of the loop should be much smaller than the wavelength. The same applies for the width of the wire (Fig. 4.2 on the left).

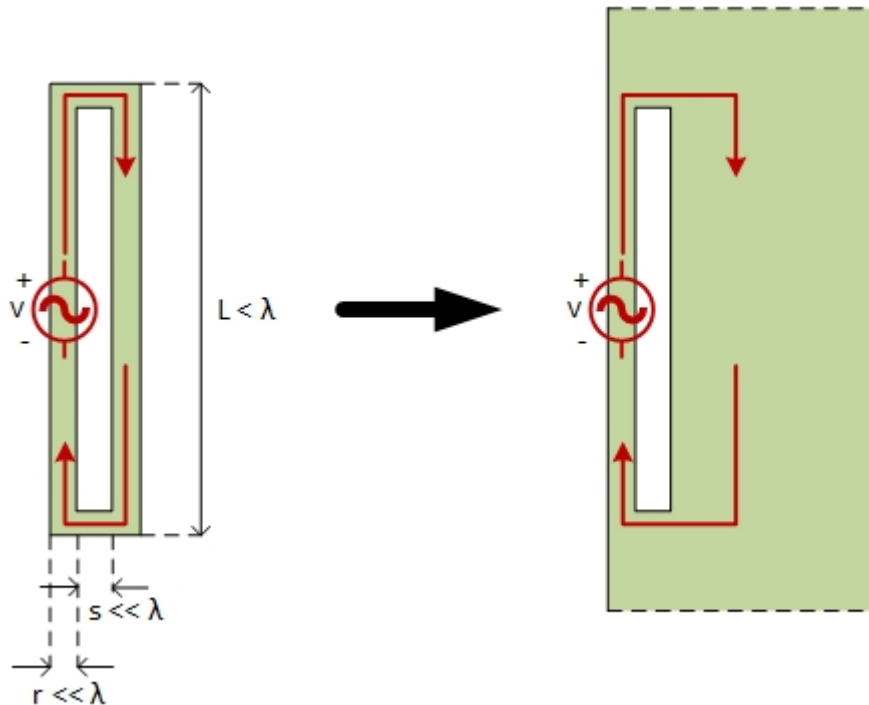


Figure 4.2: Symmetrical wire loop (left) and the non-symmetrical integrated coupling element at the edge of the patch (right)

If this wire loop is embedded at the edge of antenna plate, one of the loop arms gets much wider. Nevertheless, the strongest currents occur on the inner edge of the slot, so their electric field is cancelled in the far-field. However, current distribution will spread further, directed to the middle of the plate. A part of this current will contribute to the excitation of modal current on the plate's surface (Fig. 4.2 on the right).

### 4.3 Capacitive coupling elements

Optimal location for the capacitive coupling elements is in the maxima of electric field distribution, resp. in the minima of current distribution. Usually, the placement of CCE for all modes is in the corners of the antenna plate. Figure 4.3 depicts the principle of capacitive coupling elements.

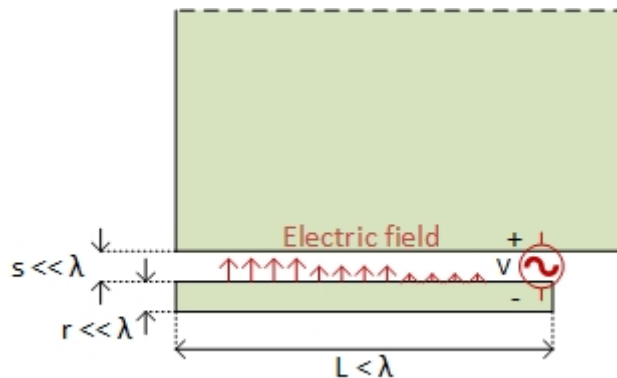


Figure 4.3: Non-resonating coplanar capacitive coupling element in the corner of the patch

The same rules apply here as for the ICE. The size of the coupling element should be small enough (much smaller than wavelength), so its contribution to radiation pattern would be insignificant. However, the specific placement of these elements enables the excitation of the required characteristic modes.

### 4.4 Excitation by coupling elements

For simulation purposes, a patch antenna was designed, which is going to work effectively around the resonance frequency  $f_c = 1,5 \text{ GHz}$ . On the patch two different modes, which are degenerative, are excited. They resonate at the same frequency, but have opposite polarization. Because of this reason, a symmetrical square patch antenna was used. The dimensions of the patch can be determined from the wavelength. The wavelength can be computed from the expression

$$\lambda = \frac{c}{f_c}, \quad (6)$$

where

- $\lambda$  is the wavelength,
- $c$  is the speed of light and
- $f_c$  is the resonance frequency.

In this case, the wavelength is  $\lambda = 0,2 \text{ m}$ . The antenna is resonating effectively, if its dimensions are half of the wavelength. So the final size of the patch is 10x10 cm.

First, it is necessary to identify, which modes occur on the analyzed patch. The MATLAB program, which is provided by the Department of Electromagnetic Field, is a powerful tool for this. The program consists of more parts, there are different scripts for generating the geometry and for the analysis of the characteristic modes. For a trustworthy analysis, it is necessary to generate a properly dense mesh in the geometry. The number of triangles should be in the interval 500-2000. For higher number of triangles, the simulation takes too much time, for less triangles the mesh is unevenly distributed.

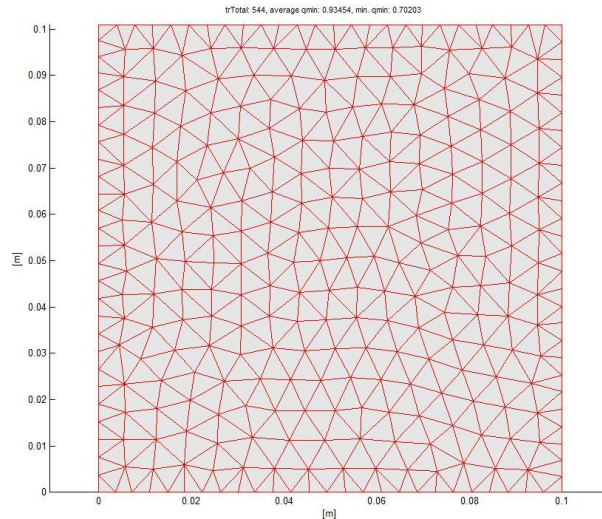


Figure 4.4: The generated mesh of the original patch

Figure 4.4 shows how the generated mesh looks like. The number of triangles is 544, which is sufficient for a correct analysis. The next figures depict the modes, which can be excited on the patch. The figure of characteristic angles (Fig. 4.5) and the figure of eigenvalues (Fig. 4.6) provides basically the same information about characteristic modes, but the characteristic angles are easier to read and interpret.

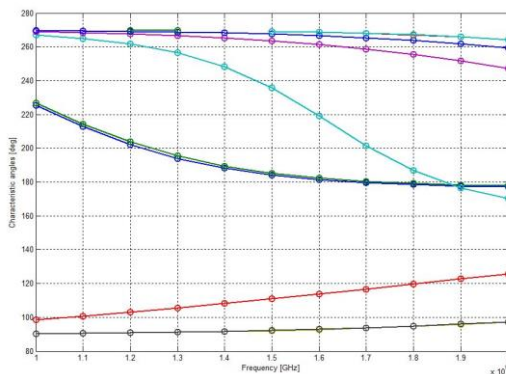


Figure 4.5: Characteristic angles, original patch

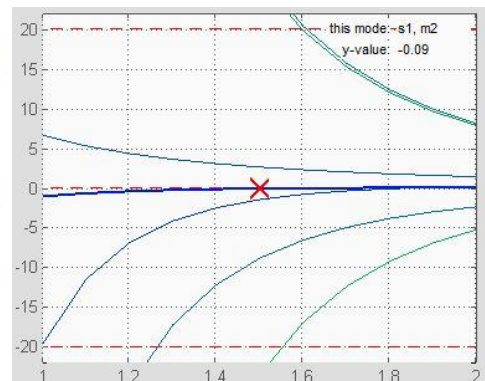


Figure 4.6: Eigenvalues of the modes, original patch

It can be seen, that at least 8 orthogonal modes can be excited on the antenna patch. From these modes, the first three is going to resonate in the frequency band 1-2 GHz. It can be observed, that the first two modes are degenerative, they are resonating at the same frequency, nevertheless they are oppositely polarized. Let's call these modes  $J_1$  and  $J_2$ . From the figures it can be read that the resonant frequency of these modes is a bit higher, it's around 1.7 GHz. However, the eigenvalues of these modes are close to zero at required frequency 1.5 GHz as well. The characteristic angles are around 185 degrees.

The third mode resonates at the frequency 1.87 GHz, but this mode is not taken into account.

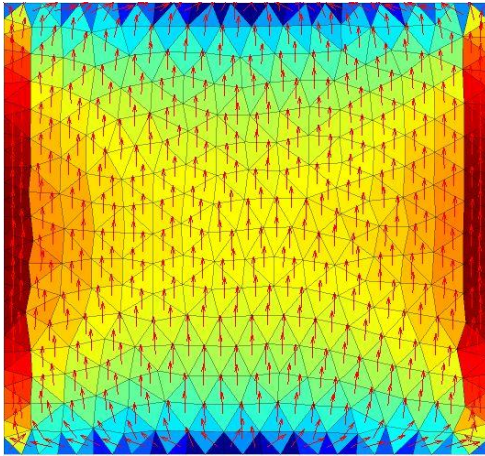


Figure 4.7: Original patch – mode  $J_1$

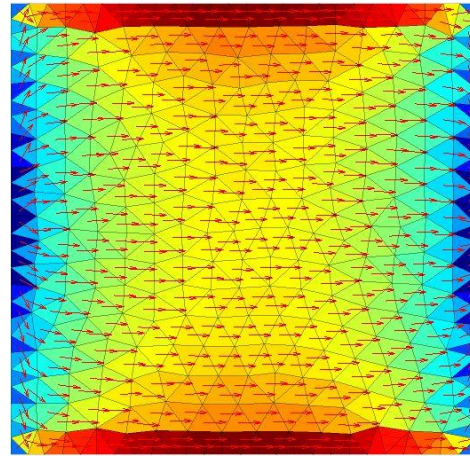


Figure 4.8: Original patch – mode  $J_2$

On the Fig. 4.7 and 4.8 the current distribution for the first two degenerative modes is illustrated. It can be easily observed, that these modes are practically identical, they only have different polarization. This can be explained by the symmetry of the patch antenna.

#### 4.5 Excitation by ICE

The next task is to excite modes  $J_1$  and  $J_2$  with a suitable method, so by using the coupling elements described above. One of the possibilities is the use of inductive coupling elements.

The geometry of the patch antenna needs to be changed. The inductive elements can be made by cutting out the slots with Boole operations. These slots should be placed where the current distribution of modes  $J_1$  and  $J_2$  has its maxima. The final mesh looks as it is shown on Fig. 4.9.

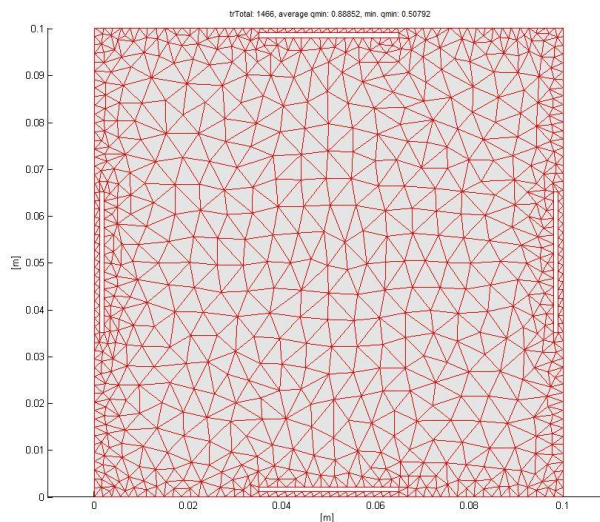


Figure 4.9: The generated mesh, ICE

Because the shape of the patch became more complex, it is necessary to use more triangles when generating the mesh. The patch should be more segmented especially around the slots. The mesh consists of 1466 triangles.

The size of the slots is determined in a manner that their width is much smaller than the wavelength ( $s = 1 \text{ mm} \ll \lambda$ ). The length of the slots is 30 mm and they are positioned at 1 mm distance from the edge of the patch. The dimensions are similar to ones found in [18]. The particular dimensions are showed in Fig. 4.10.

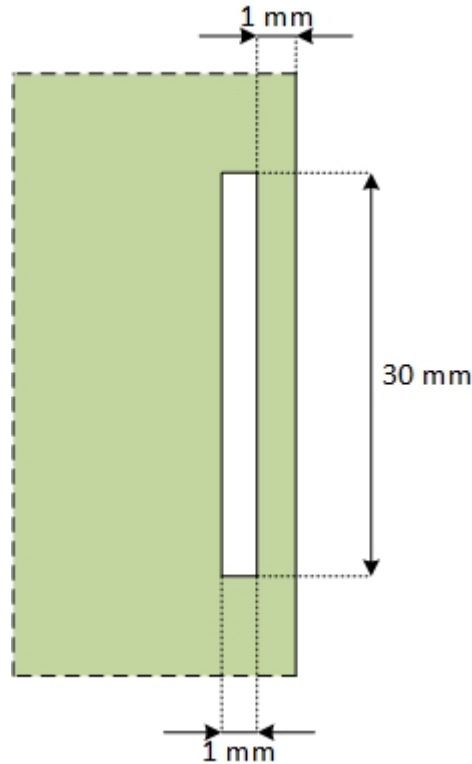


Figure 4.10: The dimensions of the coupling slots

After the calculations, it can be derived from the characteristic angles (Fig. 4.11) and eigenvalues (Fig. 4.12), that the resonant frequency for modes  $J_1$  and  $J_2$  hasn't changed. It is approximately the same what was in the case of the patch without the slots.

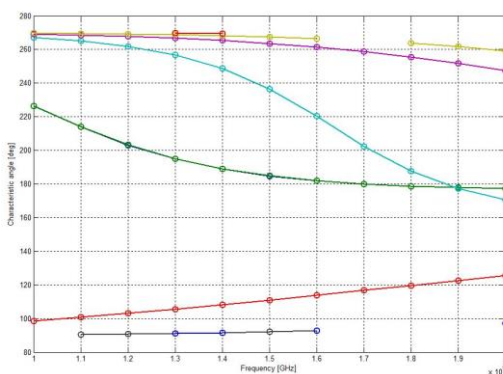


Figure 4.11: Characteristic angles, ICE

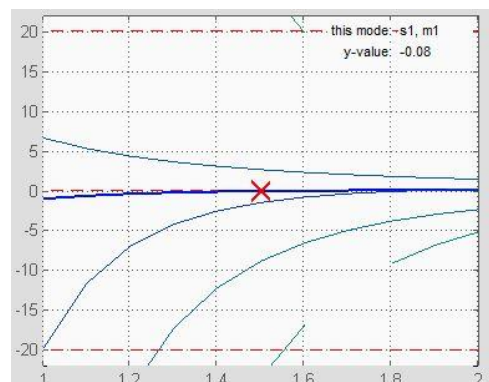


Figure 4.12: Eigenvalues, ICE

The graphs of characteristic angles and eigenvalues don't need to be continuous, because during calculations the program can switch the order of individual modes. At the end, a sorting algorithm is needed to arrange the modes to the original order. This can be



the reason, why some modes in the Fig. 4.11 and 4.12 aren't continuous or have different colors at various frequencies.

Figures 4.13 and 4.14 are illustrating that the current distributions on the surface of the patch are much more overfilled and complex. The reason is the increased amount of triangles used for simulation. It can be observed that modes  $J_1$  and  $J_2$  are still present and almost unchanged, so the inductive coupling elements can be successfully used to excite these modes.

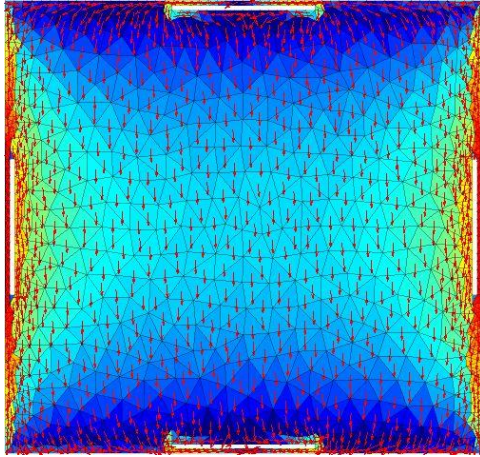


Figure 4.13: ICE – mode  $J_1$

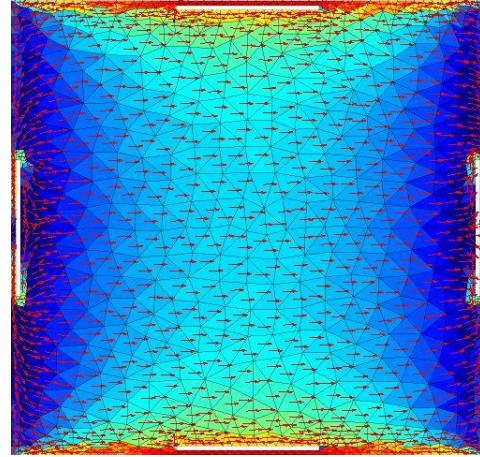


Figure 4.14: ICE – mode  $J_2$

## 4.6 Excitation by CCE

Another way to selectively excite modes  $J_1$  and  $J_2$  is by applying capacitive coupling elements. These elements need to be placed there, where the current distribution of the modes has its minima, resp. the electrical field is maximal. These places are in the corners of the patch. The original patch geometry needs to be supplemented with short conductive lines positioned to mentioned places. Four pairs of short lines will be needed, meaning eight lines together. The reason to this is, that the current distribution of modes has minima at two different locations. These locations are at both ends of each edge of the antenna patch.

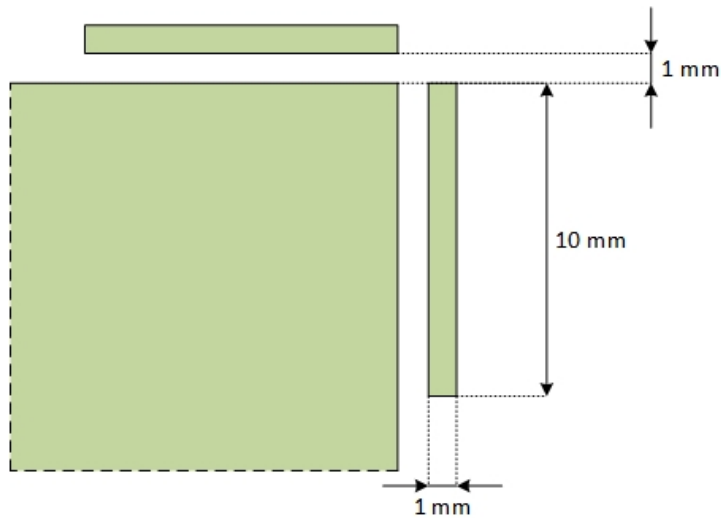


Figure 4.15: The dimensions of the capacitive coupling elements

The size of the CCE is chosen according to [22]. The width of the line is 1 mm, the length is 10 mm. The distance between the lines and the patch is also 1 mm. The situation is illustrated in the Fig. 4.15.

Figure 4.16 shows the generated mesh. The patch is segmented into 1299 triangles, so the mesh is complex enough for the trustworthy analysis.

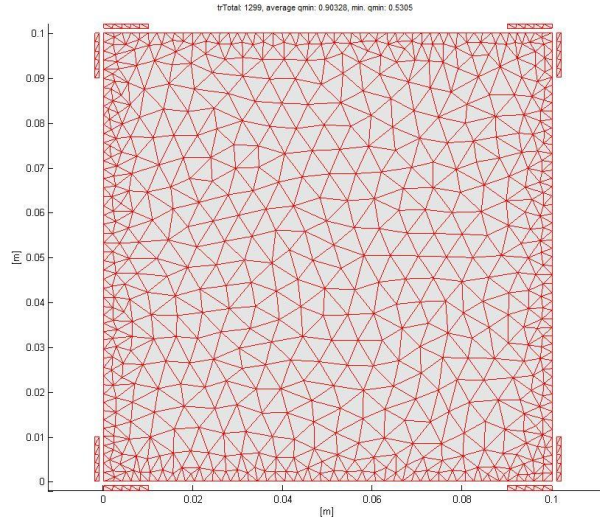


Figure 4.16: The generated mesh, CCE

The resonant frequency of the modes  $J_1$  and  $J_2$  can be determined from the results. It can be read from the graph of characteristic angles (Fig. 4.17) and graph of eigenvalues (Fig. 4.18). Final resonant frequency is also around 1.7 GHz. Here can be observed again that the graphs for higher modes are not continuous.

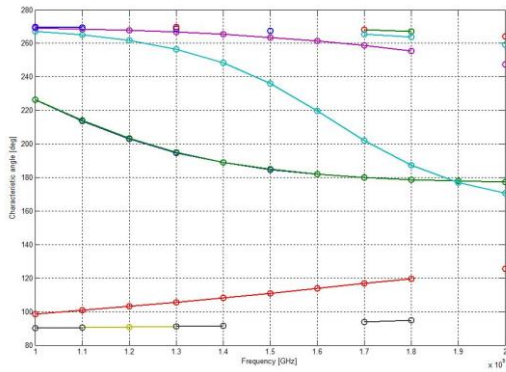


Figure 4.17: Characteristic angles, CCE



Figure 4.18: Eigenvalues, CCE

Next, Fig. 4.19 and 4.20 show the current distribution on the surface of the patch antenna for the first two characteristic modes. It can be seen, that next to the ICE capacitive coupling elements are a good solution as well for exciting the selected modes without changing their distribution on the antenna surface.

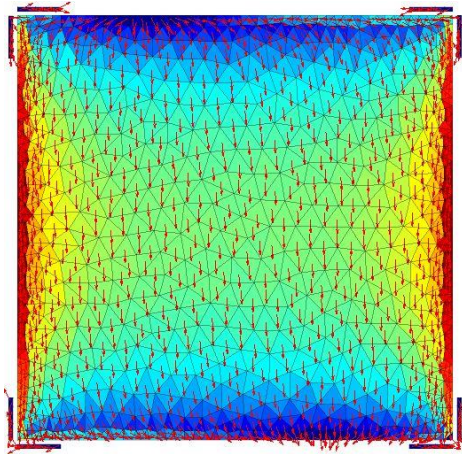


Figure 4.19: CCE – mode  $J_1$

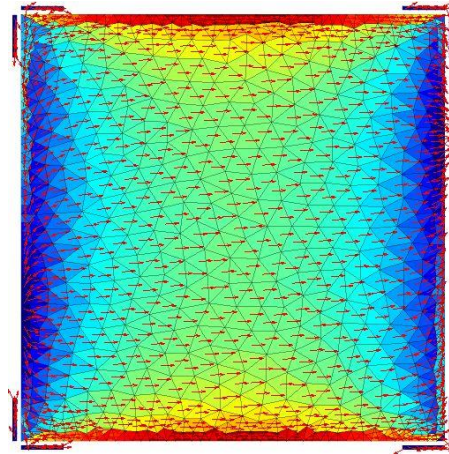


Figure 4.20: CCE – mode  $J_2$

## 4.7 Radiation patterns

Furthermore, this thesis aims to determine the radiation pattern of the patch antenna for each configuration. This can be done in the MATLAB simulation environment and with the CST software, too.

In MATLAB, there is a script available from the department, which can generate the radiation pattern from the data obtained from the characteristic mode analysis.

In CST Design Environment, the task is a bit more complicated. Each setup should be first correctly modelled and ports should be connected to specified locations to simulate the excitation.

For the ICE case, the simulation setup is depicted in the Fig. 4.21. It is necessary to connect discrete ports to the modelled antenna in a way so that each pair of the ports would be in the same phase. For two modes  $J_1$  and  $J_2$  two pairs are needed, this means four ports together. The simulation is performed selectively. Firstly, ports 1 and 2 exciting mode  $J_1$  are powered before the same is done to ports 3 and 4 which are exciting mode  $J_2$ .

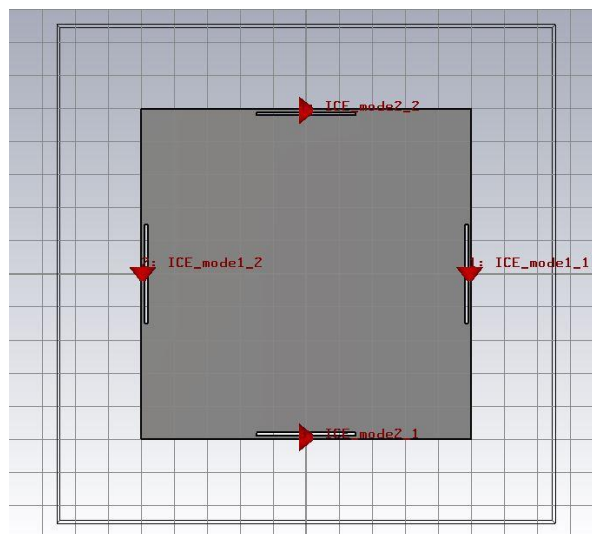


Figure 4.21: The ICE model in CST with the connected discrete ports

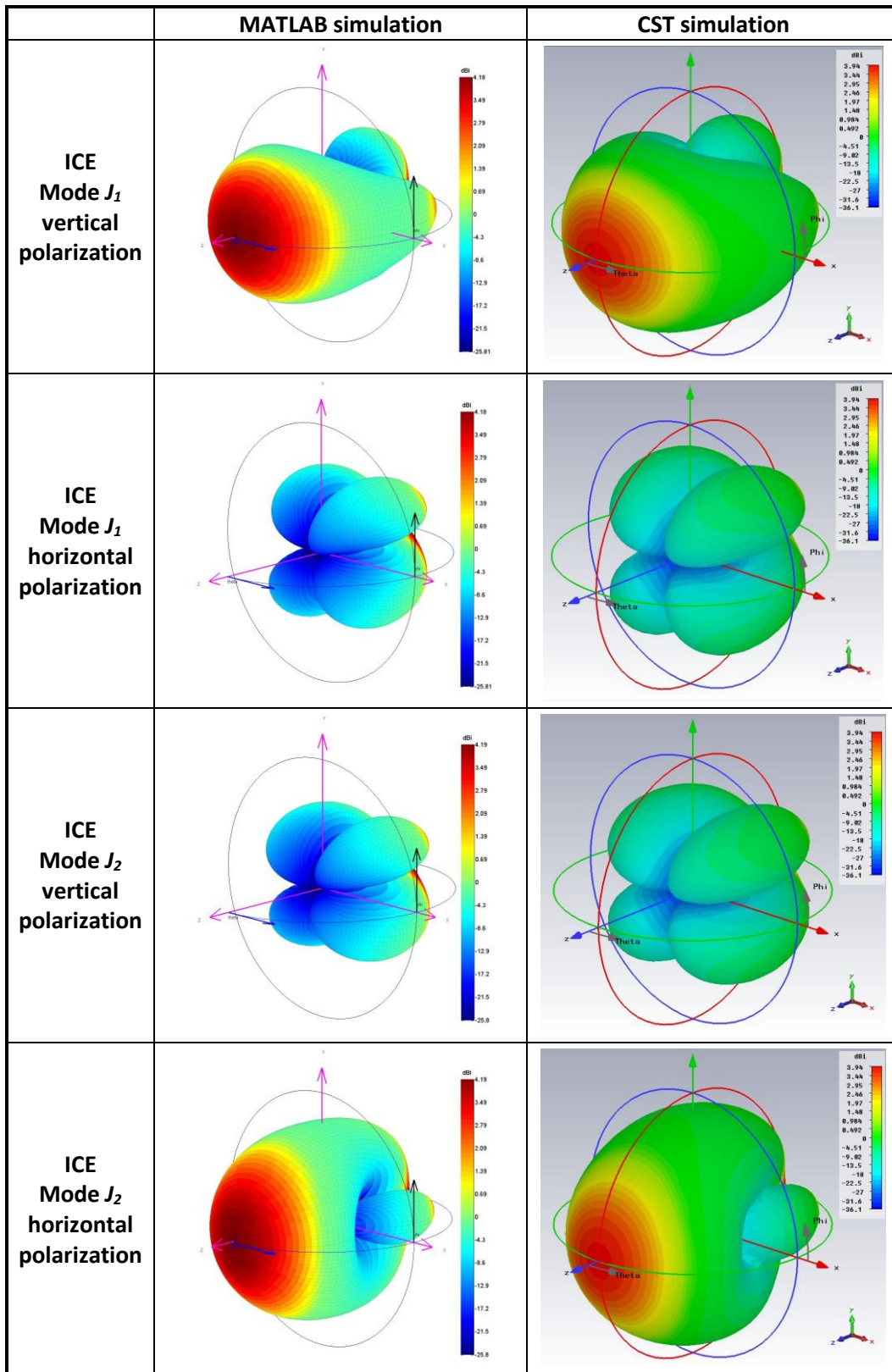


Table 4.1: The comparison of the 3D radiation pattern diagrams for ICE model

It can be observed from the Tab. 4.1, that both radiation patterns, made either by MATLAB or CST, are almost identical. It can be seen moreover, that modes  $J_1$  and  $J_2$  are truly degenerative. Both simulations confirmed this fact. The maximum directivity is 4.19 resp. 3.94 dBi. This difference is small enough, so the radiation patterns are comparable.

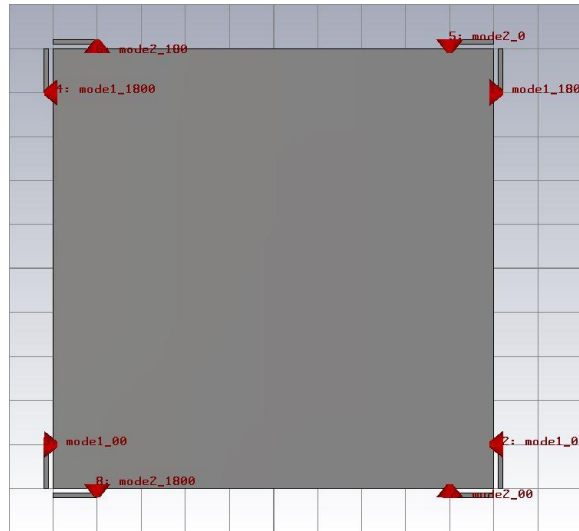


Figure 4.22: The CCE model with connected discrete ports

For the CCE case, the situation is similar, although more ports need to be used. For the excitation of one mode four ports are required. The port pairs on one edge of the patch must be powered in opposite phase to successfully excite desired modes  $J_1$  and  $J_2$ . The layout of the ports is shown in the Fig. 4.22. Ports 1, 2, 3 and 4 excite mode  $J_1$  and ports 5, 6, 7 and 8 excite mode  $J_2$ .

	MATLAB simulation	CST simulation
ICE Mode $J_1$ vertical polarization		
ICE Mode $J_1$ horizontal polarization		

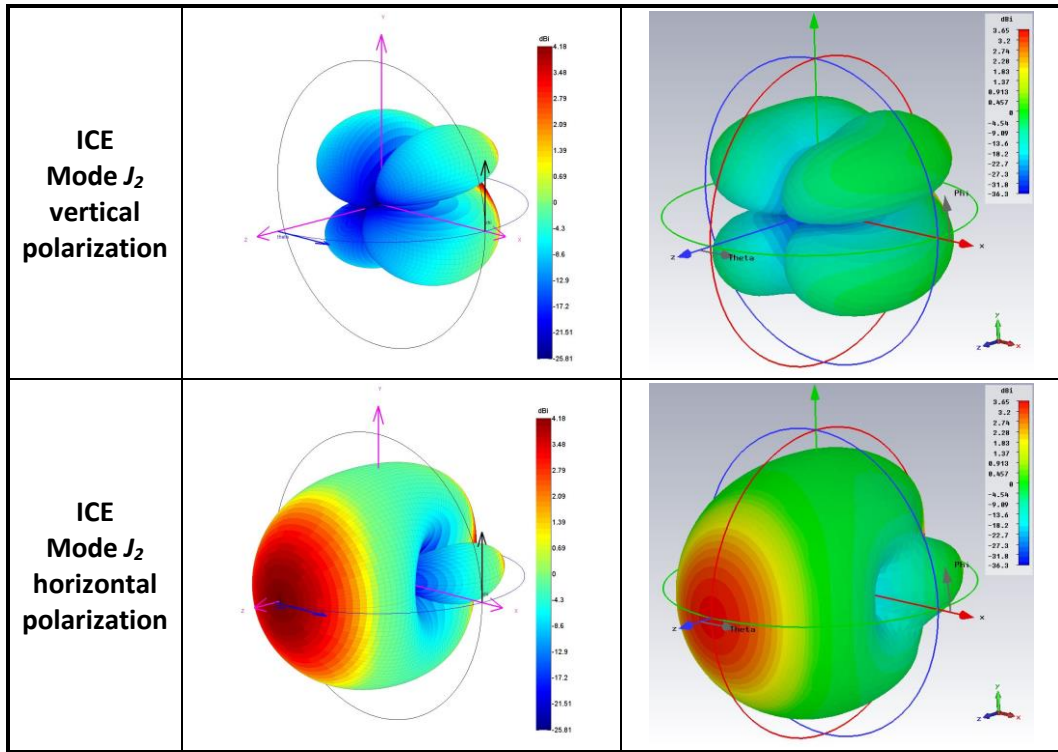


Table 4.2: The comparison of 3D radiation pattern diagrams for CCE model

The Tab. 4.2 contains the radiation patterns for both simulations. The maximum achievable directivity is 4.18 dBi for MATLAB simulation and 3.65 dBi for CST simulation. It can be witnessed, that the shape of the radiation pattern is not precisely equivalent, but still comparable in both cases.

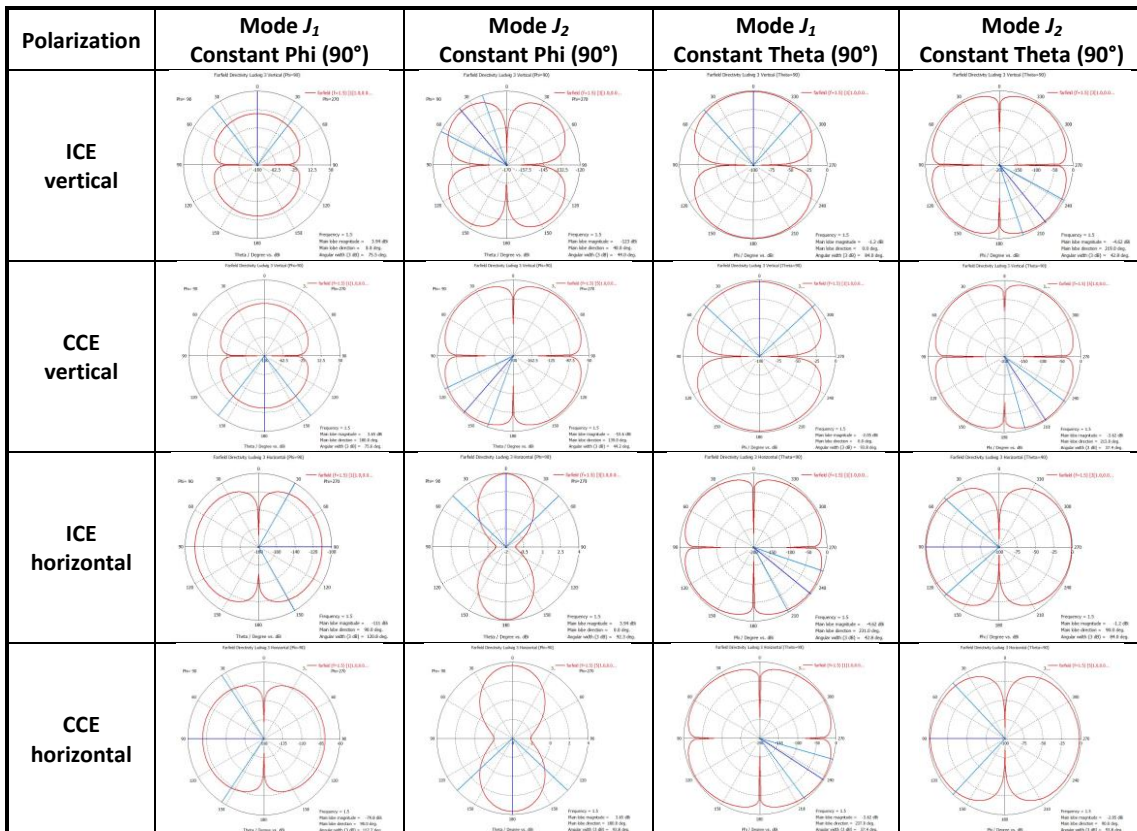


Table 4.3: The comparison of cross cut radiation pattern diagrams in CST software

## 4.8 Radiation pattern cross cut

The visual comparison of 3D radiation patterns above in decibels provides only a qualitative idea about the differences of these simulations. Better way to compare the simulation results is to put the polar forms of the radiation patterns next to each other. Unfortunately, the MATLAB script is not capable of making this form of radiation pattern. Hence only the polar diagrams obtained from CST software – for both situations – are listed here. First, the angle phi, after that the angle theta is constant. The cut angle in both cases is 90 degrees. The Tab. 4.3 is a very good way to compare the differences between ICE and CCE solution. It can be observed, that the radiation patterns differ only in small details. The same modes excited by different coupling elements have almost identical radiation patterns.

## 4.9 Impedance matching

So far, in all of the simulations the impedance matching was not taken into account. If the designed antenna wants to be used in practice, it is necessary to have the antenna input impedance matched to 50 Ω. In this work, the impedance matching will be done by lumped elements. Input impedance is calculated using the CST software. Because of symmetry, all the ports will have the same input impedance.

For designing and controlling the matching circuit, freely available online applications were used on the websites [23] and [24].

### 4.9.1 Inductive coupling elements

For the selective excitation of modes  $J_1$  and  $J_2$  by inductive coupling elements the input impedance is

$$Z_{ICE} = 16.39 + j293.22 \Omega. \quad (7)$$

This impedance has an inductive character, meaning small real part and large imaginary part. Because this impedance is the same for both port pairs, in order to connect the antenna to the 50 Ohm transmission line this impedance can be divided by two and it will be sufficient to match this half impedance.

Possible solutions for impedance matching shows the Tab. 4.4.

	$\frac{Z_{ICE}}{2} = 8.20 + j146.61 \Omega$ $L = 38.11 \text{ nH}$ $C = 1.011 \text{ pF}$
	$\frac{Z_{ICE}}{2} = 8.20 + j146.61 \Omega$ $L = 2.35 \text{ nH}$ $C = 0.643 \text{ pF}$

Table 4.4: ICE – impedance matching circuits

These matching circuits can be used for all ports of the antenna, always different circuit for every port pair.

#### 4.9.2 Capacitive coupling elements

If the first two characteristic modes are excited by capacitive coupling elements, input impedance will be

$$Z_{CCE} = 11.98 - j418.98 \Omega. \quad (8)$$

The real part of the impedance is almost the same as for the ICE situation, but the imaginary part is larger and has an opposite sign. Variations for a matching circuit are shown in the table.

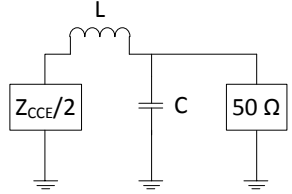
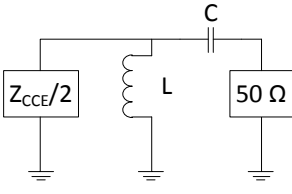
	$\frac{Z_{CCE}}{2} = 5.99 - j209.49 \Omega$ $L = 23.95 \text{ nH}$ $C = 5.752 \text{ pF}$
	$\frac{Z_{CCE}}{2} = 5.99 - j209.49 \Omega$ $L = 16.54 \text{ nH}$ $C = 0.176 \text{ pF}$

Table 4.5: CCE – impedance matching circuits

Because the input impedance is same for all ports, the same matching circuit can be used for every pair of ports.

## 4.10 Summary of the coupling elements

In this section of the master thesis the possibilities of the use of a coupling element were investigated. The excitation of the first two characteristic modes on the designed patch antenna was discussed and tested. These two modes,  $J_1$  and  $J_2$  are degenerative modes. Because of this, these modes can be excited in different polarization giving the patch antenna the possibility to be used in MIMO systems.

Two types of coupling elements were used. First, small slots were cut at the edges of the patch. This solution represents the inductive coupling elements. Secondly, small lines were attached to the antenna in the corners of the patch. This method uses capacitive coupling elements.

By comparing the radiation pattern, both in MATLAB and CST software, it can be declared, that both solutions are an appropriate way to excite required characteristic modes on the patch. The differences are negligible, nevertheless, with some more research even these small differences can be corrected.

At the end of this chapter, two kinds of impedance matching circuits were designed for each solution method. The input impedance of the designed antenna was matched to the output impedance  $50 \Omega$ .



## Chapter 5

# L-probe feeding system

### 5.1 Introduction

In this part of the work, a different feeding technic, the so called “L-probe” is used [25]. A square patch antenna is designed, simulated and measured. Firstly, the principle and the physics behind the method is presented. After that, the modeling process is described in details, so a number of parameter sweep simulations are executed in CST software to find how different parameters effect the whole structure and radiation properties. Finally, the antenna with the parameters, which were proven to be the best, is fabricated and measured in the anechoic chamber. The results are investigated and compared with the simulation. At the end, the differences are discussed.

### 5.2 L-probe systems

The name of the L-probe feeding system came from the shape of the exciter, which is a metallic wire resembling the shape of the letter L. This system is a relatively new feeding method in microstrip patch antennas [26], [27]. It enables a higher emplacement of the patch antenna over the ground plane – usually over  $0.1\lambda$  – resulting in greater impedance bandwidth. The principle of the L-probe system is shown in Fig. 5.1. From this figure is evident, that the discussed L-probe feeding system is basically a different type from the group of capacitive coupling elements.

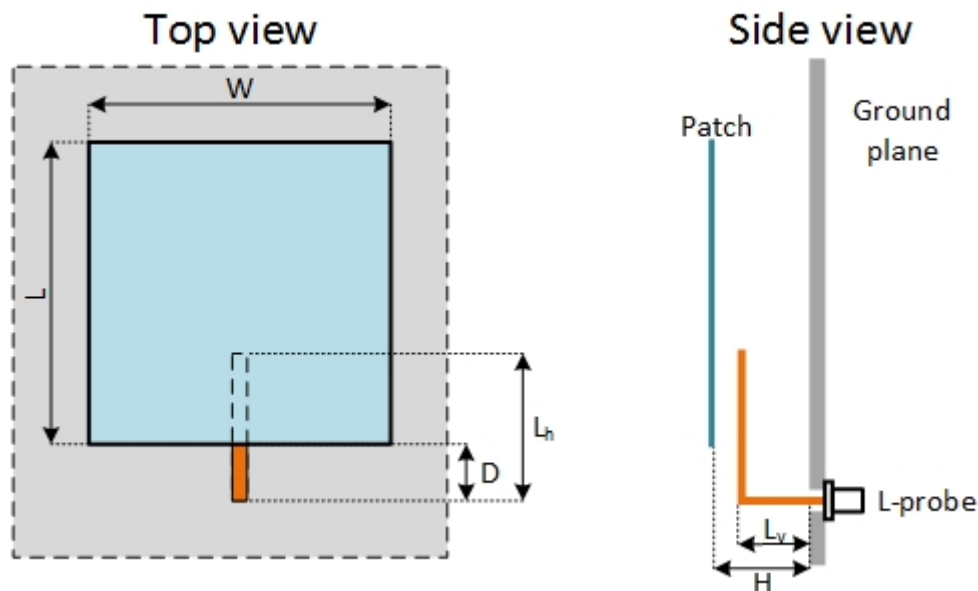


Figure 5.1: The principle of the L-probe system

The notations in the figure are the following:

- $L$  is the length of the patch antenna
- $W$  is the width of the patch antenna
- $H$  is the height, where the patch antenna is positioned over the ground plane

- $L_v$  is the length of the vertical part of the L-probe
- $L_h$  is the length of the horizontal part of the L-probe
- $D$  is the difference between the position of the vertical part of the L-probe and the patch edge

The main advantages of the L-probe feeding system are [25]:

- higher impedance bandwidth than the other feeding methods (up to 40%),
- more freedom in the antenna design,
- high radiation efficiency (90% a more) thanks to the missing surface waves,
- relatively flat character of the gain,
- predictable behavior of the radiation pattern,
- simple and cost efficient production, no need for a substrate,
- non-destructive assembly (no need to drill into the patch, etc.),
- parameters are less resistant against the manufacturing tolerances.

### 5.3 Equivalent circuit

The L-probe feeding system could be viewed as a capacitively loaded monopole electromagnetically coupled to the  $TM_{01}$  mode field under the patch. The patch antenna can be modelled as parallel RLC circuit and the L-probe as a stub consisting of two ideal lines. Other elements are representing the parasitic components, shown in Fig. 5.2.

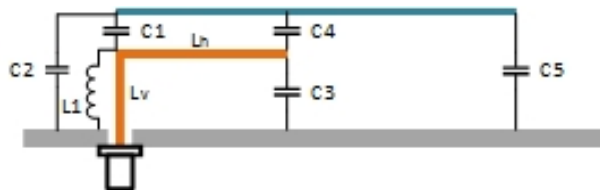


Figure 5.2: Parasitic components

As it can be seen from Fig. 5.2, the parasitic capacitors are present between the patch and the ground plane at both ends of the patch; there are capacitors between the patch and the horizontal part of the L-probe and between the ground plane and the L-probe. There is also an inductor coupled to the vertical part of the L-probe.

### 5.4 The design process

In [28], a study of a dual-polarized L-probe patch antenna is presented. They constructed a square patch antenna with four L-probes. Each pair of these L-probes is excited with  $180^\circ$  phase difference. They present a new feeding system, with which an isolation over 30 dB can be achieved.

In another study [29], the high bandwidth and isolation is achieved by using a novel  $180^\circ$  broadband microstrip balun, which delivers balanced power splitting and phase shifting over a wide band. This antenna also uses two pairs of L-probes placed against each other.

After studying the above mentioned papers came the idea of designing a square patch antenna, which has four L-probes as well, but instead exciting them all, only two will be fed through N-connectors, and the other two on the opposite side will act as a parasitic L-probe. This chapter describes the design process of such an antenna.

For finding the best design, number of parameter sweeps were executed. The starting points were recommendations from [30]. In that work, the following dimensions were determined through experiments for optimal performance:

- For the design of the patch
  - o The resonant length of the patch is

$$L = \frac{c}{f_c} \frac{3}{8} \quad (9)$$

This equation takes into account the fringing field effect and the fact that resonance has to be shifted below the center frequency to obtain broadband behavior. In our case, the experiment simulations show that it is better to use length closer to  $\lambda/2$ .

- o The width of the patch is not a crucial design parameter, however the optimal value is

$$W = \frac{2}{3}L \quad (10)$$

Due to the fact that the designed antenna in this thesis will be a square antenna for symmetry reasons, this parameter is not used.

- The optimal L-probe dimensions are
  - o  $L_h \approx 0.15 \lambda$
  - o  $L_v \approx 0.10 \lambda$
  - o  $H \approx 0.15 - 0.18 \lambda$
  - o  $D = 0$
  - o It can be observed, that  $L_v + L_h \approx \lambda/4$ . This corresponds to the fact, that the L-probe resonates like a  $\lambda/4$  monopole.

## 5.5 Parameter sweep simulations

According to [25], a number of parameter sweep simulations were performed to find the relation between the lengths of elements. The conclusions of these simulations are listed here. The results in graphical representation can be found in the appendix (Ap. 1-3).

- The aim of the first simulation was to find the optimal width of the patch and its position over the ground plane. Five heights and five patch widths were investigated. The height  $H$  was chosen from the interval 24-32 mm with step size 2 mm. For each height a patch width is assigned from the interval 85-105 mm with step size 5 mm. The other parameters are:
  - o  $L_v = 20 \text{ mm}$
  - o  $L_h = 32 \text{ mm}$

From the Ap. 1 it can be observed, that the parameter  $H$  changes the S-parameter  $S_{11}$  as follows: with higher  $H$ , the central resonance frequency is shifted towards higher frequencies. In the Smith-diagram parameter  $H$  effects the size and the shape of the loop. The change in the patch width effects mostly the magnitude of the return loss parameter.

- The second simulation focuses on the connection between the patch height  $H$  and the length of the horizontal part of the L-probe  $L_h$ . The parameter  $H$  is selected in the same way as before, so from the interval 24-32 mm with step size 2 mm. The

size of the horizontal component of the L-probe changes between 26 and 38 mm with step size 3 mm for each height. The other parameters are constant:

- o  $L_v = 20 \text{ mm}$
- o  $W = 95 \text{ mm}$

According to Ap. 2, the role of the parameter  $H$  is the same as in the first simulation: higher  $H$  moves the resonant frequency upwards and changes the size and shape of the loop in the Smith-diagram. The parameter  $L_h$  effects the resonant frequency and changes the position of the loop and the size in the Smith-diagram.

- The last simulation investigates the relation between the vertical and horizontal part of the L-probe. The length  $L_v$  is chosen from the interval 18-22 mm with step size only 1 mm. For each  $L_v$  the length of the horizontal part is selected from 26 to 34 mm with step size 2 mm. The constant parameters are:
  - o  $H = 26 \text{ mm}$
  - o  $W = 95 \text{ mm}$

The results of the simulation show (Ap. 3) that these two parameters have the most critical effect on the behavior of the antenna. The parameter  $L_v$  effects the size of the loop in the Smith-diagram. The higher  $L_v$  shifts the resonant frequency to the lower frequencies. The parameter  $L_h$  effects not only the position, but also the size of the loop in the Smith-diagram. Just as in case of  $L_v$ , the higher  $L_h$  also moves the resonant frequency lower and effects the return loss parameter.

## 5.6 The designed antenna

After evaluating the results from the previous parameter sweep simulations, the optimal dimensions of the proposed antenna were selected. The dimensions were chosen in a manner that the required resonant frequency  $f_c = 1.5 \text{ GHz}$  would be in the middle of the frequency band. The selected parameters are shown in the Tab. 5.1.

Parameter	Size [mm]	Size compared to $\lambda$
$H$	27	$0.135 \lambda$
$W$	95	$0.475 \lambda$
$L_h$	32	$0.16 \lambda$
$L_v$	20	$0.10 \lambda$
$D$	5	$0.025 \lambda$

Table 5.1: The parameters of the designed antenna

The dimensions and the layout of the antenna from the top and the side view is depicted on the Fig. 5.3. The dimensions are in millimeters.

The designed antenna has two input ports which are fed through N-type connectors. The other two L-probes have no feeding mechanism, they are parasitic and shorted at the ground plane. Their effect and properties will be investigated in simulations.

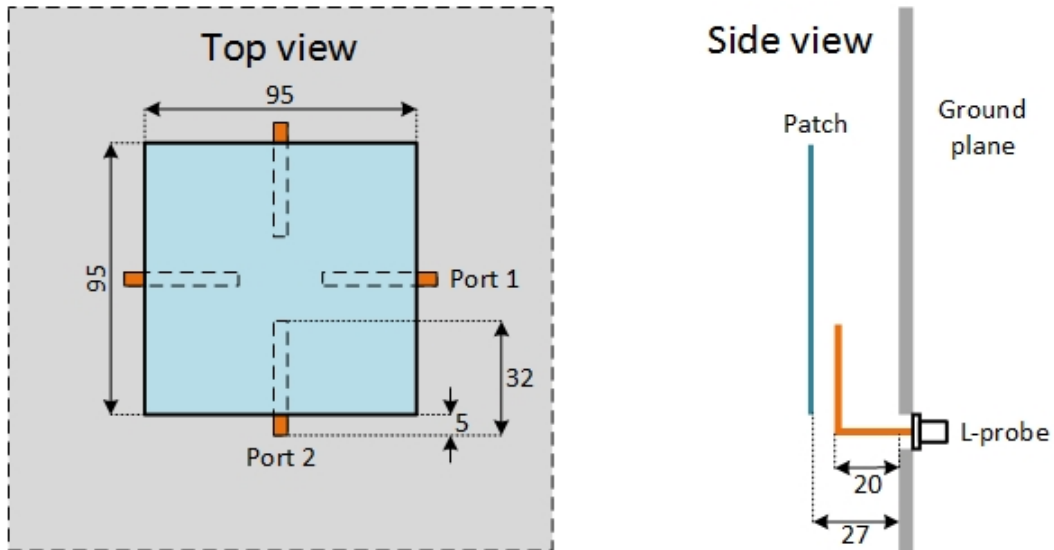


Figure 5.3: The parameters and the layout of the designed antenna (dimensions in mm)

## 5.7 Properties of the designed antenna

The designed antenna was simulated in CST software (Fig. 5.4). The finite ground plane has dimensions 286x286 mm. In this section, the properties of the antenna like return loss, isolation, envelope cross-correlation, etc. are calculated and listed.

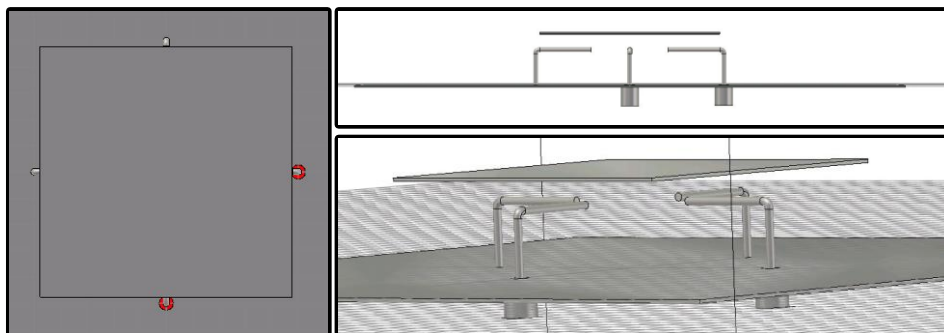


Figure 5.4: The designed antenna model in CST

Figure 5.5 shows the parameters  $S_{11}$  and  $S_{22}$ , the so called return loss. The parameters are identical both for port 1 and port 2, because of the symmetry of the layout. The middle frequency is 1.5 GHz and the antenna has lower return loss than -10 dB from 1.3 GHz to 1.7 GHz. The relative bandwidth can be calculated according to [25] with the help of the following equation:

$$BW = \frac{f_2 - f_1}{f_c} \cdot 100 [\%]. \quad (11)$$

Where

- $f_1 = 1.3 \text{ GHz}$ ,
- $f_2 = 1.7 \text{ GHz}$  and
- $f_c = 1.5 \text{ GHz}$ .

So, the relative bandwidth for  $|S_{11}| = |S_{22}| < -10 \text{ dB}$  is 26.67 %. This wide bandwidth is achieved thanks to the L-probe feeding system.

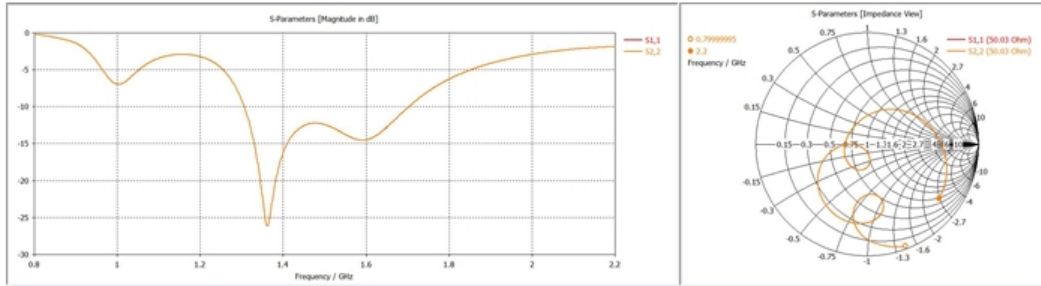


Figure 5.5: The return loss parameter ( $S_{11}$  and  $S_{22}$ ) of the designed antenna

From Fig. 5.5, another resonance can be observed at the frequency 1 GHz. This is the resonance of the parasitic L-probe, which is located opposite to the excited port. It can be observed also from the Smith-diagram, where the second loop represents this parasitic element. Despite the fact that in this thesis the idea is not applied, this parasitic resonance can be used in a profitable way as well. It can be considered as a possibility to enhance the bandwidth. With proper modification and refining, the two resonances can be shifted nearer to each other producing a wider relative bandwidth.

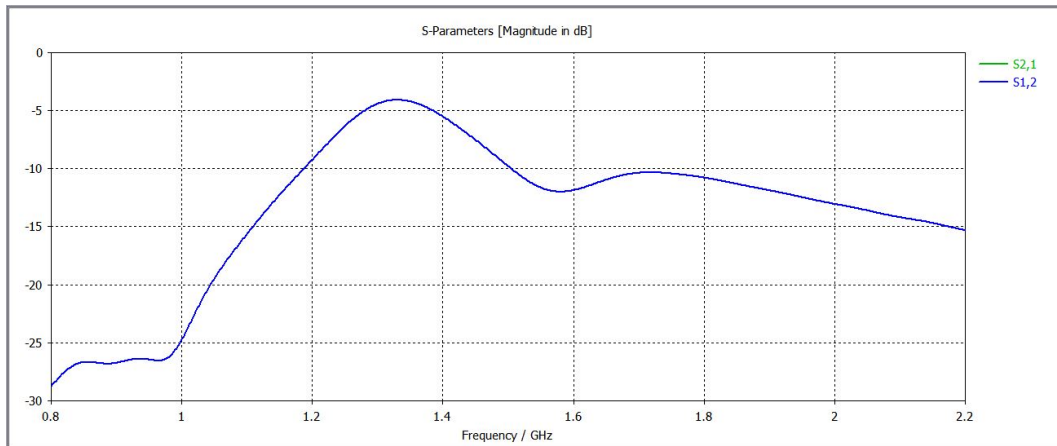


Figure 5.6: The isolation ( $S_{12}$  and  $S_{21}$ ) between the ports

The S-parameter  $S_{12}$  or  $S_{21}$ , the so called isolation, is not too high in this case, it is only around -10 dB for resonant frequency, which is not sufficient for mobile communication. This thesis does not focus on isolation enhancement. For further study, isolation improvement technologies can be found in [28] and [29] for L-probe systems and in [31], [32] and [33] for the MIMO systems in general. Most of these works propose an isolation technique using ground plane shape modifications, such as cutting slots in the ground plane or making little obstacles to prevent the flow of the surface current; another possibility is excitation with  $180^\circ$  phase shifting in the feeding system.

The input impedance for both the L-probes alone and for the L-probes and the patch together was compared to each other. It has an interesting behavior. For the patch and the L-probes together, the real part is around  $50 \Omega$  in the desired band. The imaginary part oscillates around zero in a quite wide band. The reason of this is explained in [28]: there is an electromagnetic coupling between the probe and the patch, where their natural resonances are combined. This idea was also confirmed by equivalent model simulations.

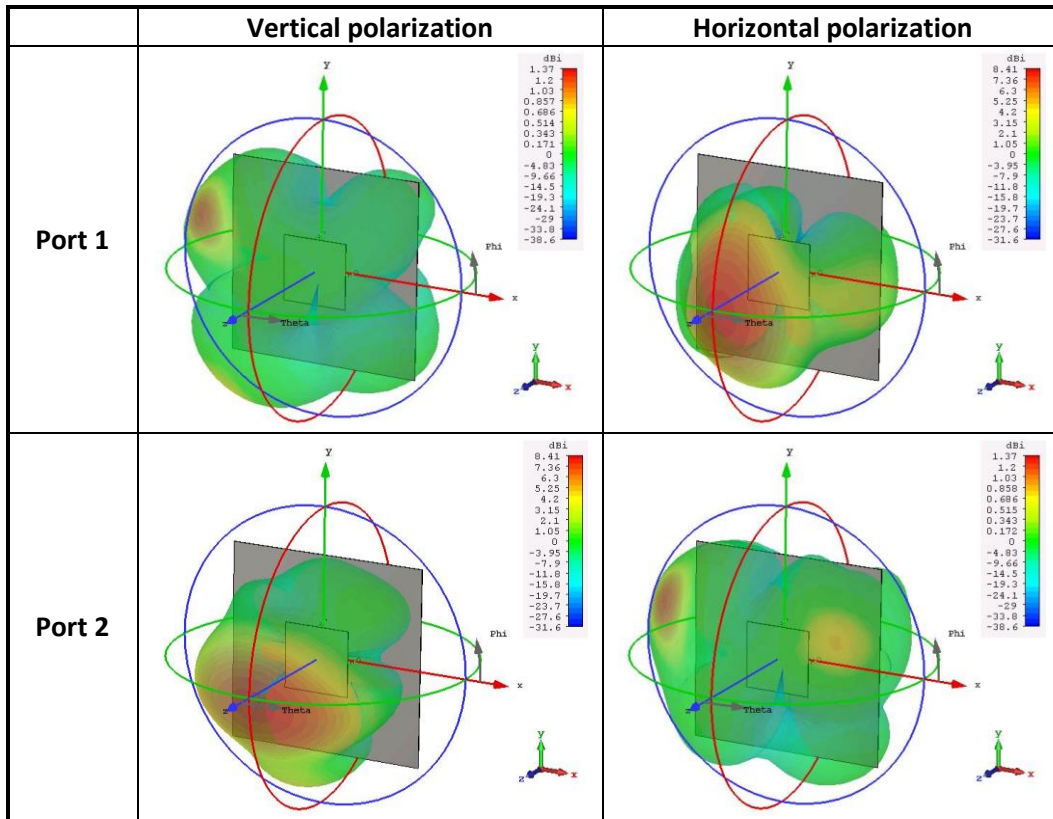


Table 5.2: 3D radiation patterns of the designed antenna

In Tab. 5.2 the 3D radiation diagrams are illustrated for both ports. Port 1 radiates mostly in horizontal polarization. The maximum achievable directivity is 8.41 dBi, in vertical polarization only 1.37 dBi. The radiation pattern is not symmetrical. The reason for this is the fact, that despite the layout and the arrangement of the L-probes is symmetrical, from the radiation perspective it is not. The parasitic L-probes are shorted at the ground plane. If one port is excited in the simulation, the other one is modelled with  $50 \Omega$  ending. This asymmetry causes the radiation not to be evenly distributed. The maximal asymmetry can be observed in minor polarizations, where part of the energy is radiated towards the opposite parasitic L-probes from the excited port. For port 2 the main polarization is the vertical polarization. This situation is confirmed in polar cut radiation diagrams (Tab. 5.3). The radiation pattern is showed in the plane where either angle phi or angle theta is constant. In the figures a 90-degree shift can be detected between the port 1 and port 2. This is a reasonable behavior; it can be traced back to the arrangement of the excited L-probes – they are rotated with respect to each other by 90-degree. Unfortunately, none of the radiation diagrams is perfectly clear regards to the polarization. They are rotated by a few degrees because of the presence of parasitic L-probes.

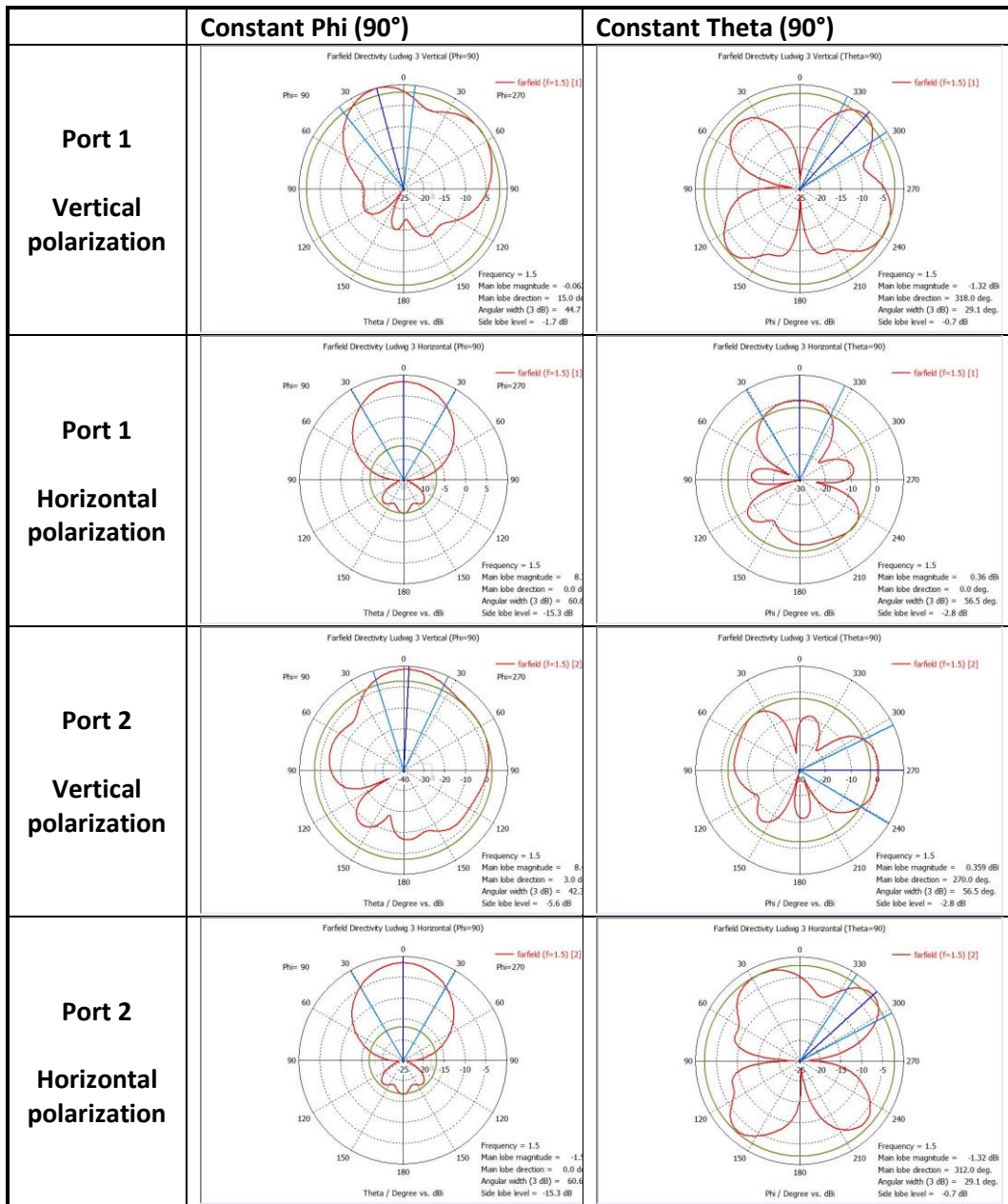


Table 5.3: Polar cut radiation diagrams of the designed antenna

Figure 5.7 shows the difference between the polarizations. Around the center frequency  $f_c = 1.5 \text{ GHz}$  it is approximately 10 dB.

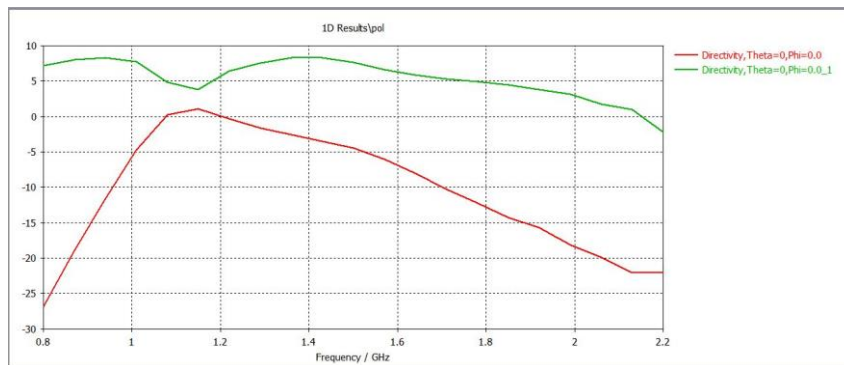


Figure 5.7: The difference between polarizations



## 5.8 Envelope cross correlation

Another interesting parameter describing the coupling between the ports is the far-field cross correlation parameter [34]. The basic idea here is to use the reciprocity theorem, which relates the far-field of transmitting antenna to its receiving characteristics. If identical elements are used for both transmit and receive arrays, and the angles of incidence of the illuminating fields are assumed to be uniformly distributed, then the degree of correlation in the receiver signals can be directly related to the cross correlation of the far-fields radiated by the elements of the transmit array. Because the designed antenna uses the polarization diversity principle, it can be considered as a MIMO configuration. This means that the above mentioned reciprocity theorem can be applied for calculating the cross correlation. Let the radiation patterns of port 1 and port 2 be  $E_1(\vartheta, \varphi)$  and  $E_2(\vartheta, \varphi)$ , respectively (in this case the two polarizations will be considered as the two radiation patterns). According to [35], the envelope cross correlation between two antennas is defined as

$$\rho = \frac{\left| \int_{4\pi} d\Omega \mathbf{E}_1(\theta, \varphi) \mathbf{E}_2^*(\theta, \varphi) \right|}{\sqrt{\int_{4\pi} d\Omega |\mathbf{E}_1(\theta, \varphi)|^2} \sqrt{\int_{4\pi} d\Omega |\mathbf{E}_2(\theta, \varphi)|^2}} \quad (12)$$

Where the integration is with respect to the full solid angle  $\Omega$ , "\*" denotes the complex conjugate operator, and  $|\mathbf{E}_{1,2}(\theta, \varphi)|^2 = \mathbf{E}_{1,2}(\theta, \varphi) \mathbf{E}_{1,2}^*(\theta, \varphi)$ .

There is another method to calculate the cross correlation. Recently, it was proposed in [36], that an exact relation exists for lossless antennas. In this relation the envelope cross correlation between two antennas can be determined uniquely through the S-parameters with the relation

$$\rho = \frac{|S_{11}^* S_{12} + S_{21}^* S_{22}|}{\sqrt{1 - |S_{11}|^2 - |S_{21}|^2} \sqrt{1 - |S_{22}|^2 - |S_{12}|^2}} \quad (13)$$

This equation has become popular because of its simplicity. It is eliminating the necessity of the difficult integral computations of the envelope cross correlation in Eq. (12). A standard measurement procedure of input parameters at the antenna terminals is sufficient. However, in [35], there is a proof that this computation method is numerically inadequate and it may occasionally work, but it is not correct in general.

Nevertheless, in this master thesis, the envelope cross correlation is computed with both of the methods and the results are compared in Fig. 5.8.

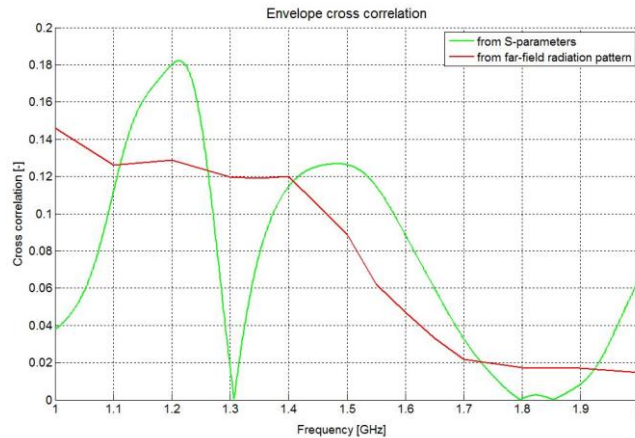


Figure 5.8: Envelope cross correlation computed with two methods

It can be seen from Fig. 5.8, that for some frequencies both of the calculation methods give more or less the same results. In the required bandwidth – so from 1.3 GHz to 1.7 GHz – the calculated envelope cross correlation values are comparable. The biggest differences are for smaller frequencies. However, because the correlation calculated from the far-field radiation pattern gives more stable result, it seems to be more trustworthy. The values of envelope cross correlation are around 0.12 for the frequencies smaller than 1.4 GHz. After that a steep drop can be observed and the envelope cross correlation decreases to 0.02 for frequencies higher than 1.7 GHz. These values are quite small which is favorable.

## 5.9 Characteristic modes of the designed antenna

The characteristic mode analysis is performed by CST software. It is a relatively new capability of the software [37], so in some cases it is not working properly yet. First, only the patch antenna is analyzed without a ground plane, so in free space. Basically, this is the same familiar patch as we had in the first part of the master thesis. The graph of the characteristic angles (Fig. 5.9) looks exactly the same as in Fig. 4.5.

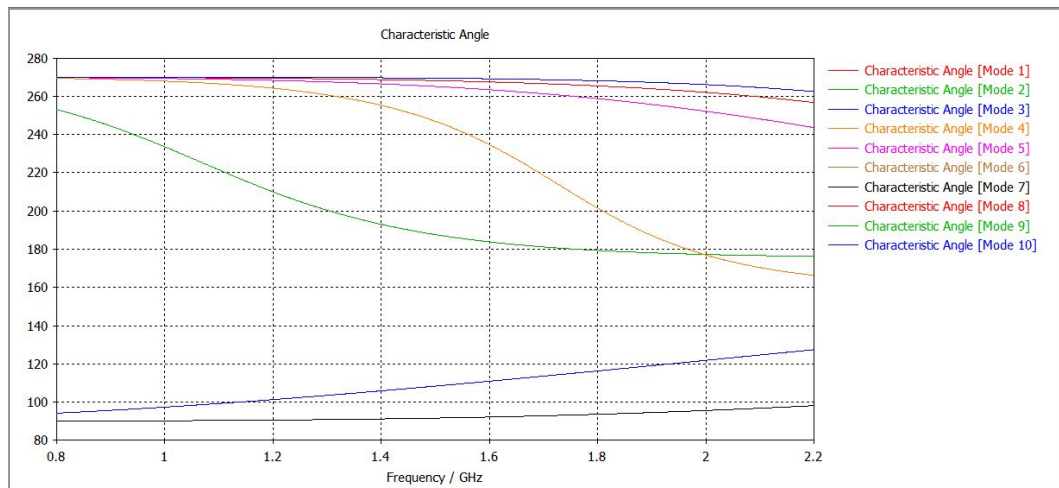


Figure 5.9: Characteristic angles of the designed antenna – patch only

The first two modes –  $TM_{10}$  and  $TM_{01}$  – are degenerative. The third mode is  $TM_{11}$  as it can be seen from Fig. 5.9 and 5.10. The third mode in Fig. 5.9 has the number 4, because the sorting algorithm of the software switched the order of the modes.

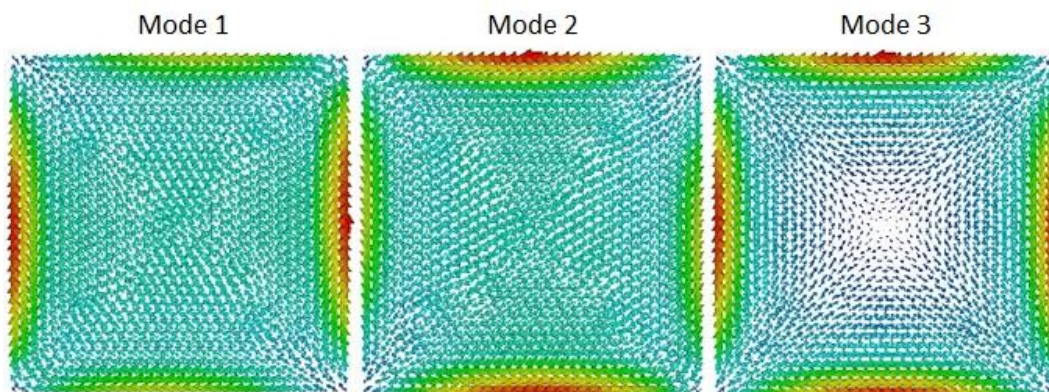


Figure 5.10: The first three characteristic modes of the patch

It is interesting to compare step by step how each element of the antenna effects the characteristic angles. Because the ground plane has finite dimensions, the modes of the patch and the modes of the ground plane are electromagnetically coupled. The characteristic angles for the patch itself are already shown above. Next, the ground plane will be examined alone. The ground plane has the size 286x286 mm. This means, that its resonance frequency will be somewhere around 520 MHz. Because of this, most of the characteristic angles in Fig. 5.11 represent the higher modes, not the dominant ones.

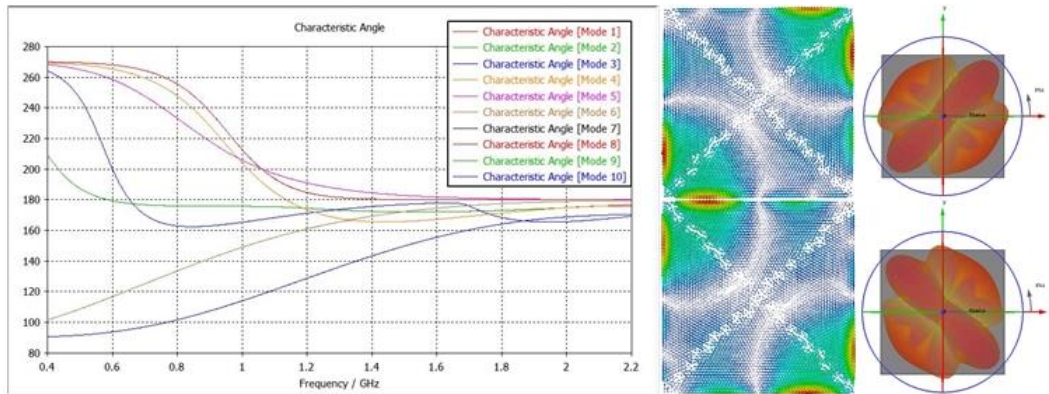


Figure 5.11: The characteristic mode analysis of the ground plane itself

The first two modes here are degenerative modes again. The surface current distribution and the radiation pattern generated by these modes is also shown in Fig 5.11. The far-field radiation pattern is calculated for 1.5 GHz.

Afterward, put the L-probes to their places on the ground plane. The results are in Fig. 5.12. Only minimal changes can be observed in the graph of characteristic angles and mostly for the higher frequencies. However, the first two degenerative modes will produce an interesting behavior. They will have a different character, they are shifted to vertical and horizontal direction. These changes can be observed in the surface current distribution as well.

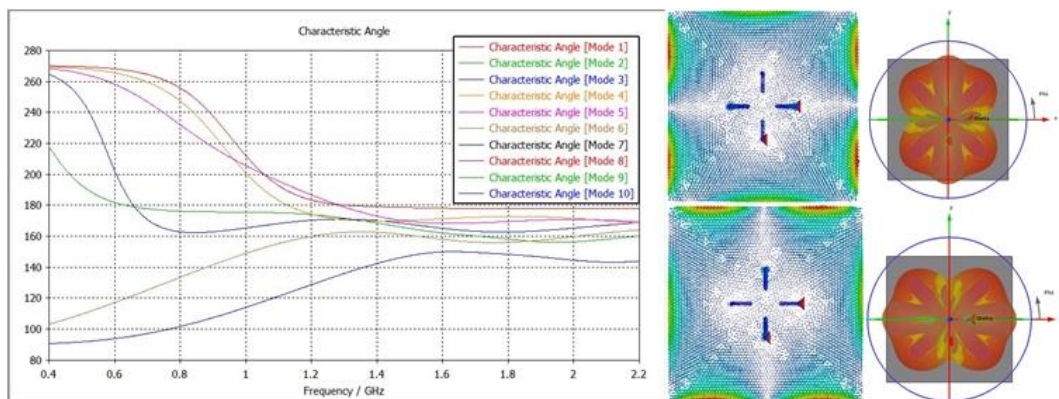


Figure 5.12: The characteristic mode analysis of the ground plane and the L-probes

At the end, the complete structure as a whole is tested. It can be seen in Fig. 5.13, that because this structure is too complex for the perfect analysis, the software has some problems with sorting the modes correctly. So, in this case it is a bit harder to find the degenerative modes. However, Mode 3 and Mode 6 show some kind of symmetry in the radiation pattern. This symmetry is not perfect, but that is reasonable, it was already observed before that the radiation patterns generated by exciting different ports show asymmetry (Tab. 5.2 and 5.3).

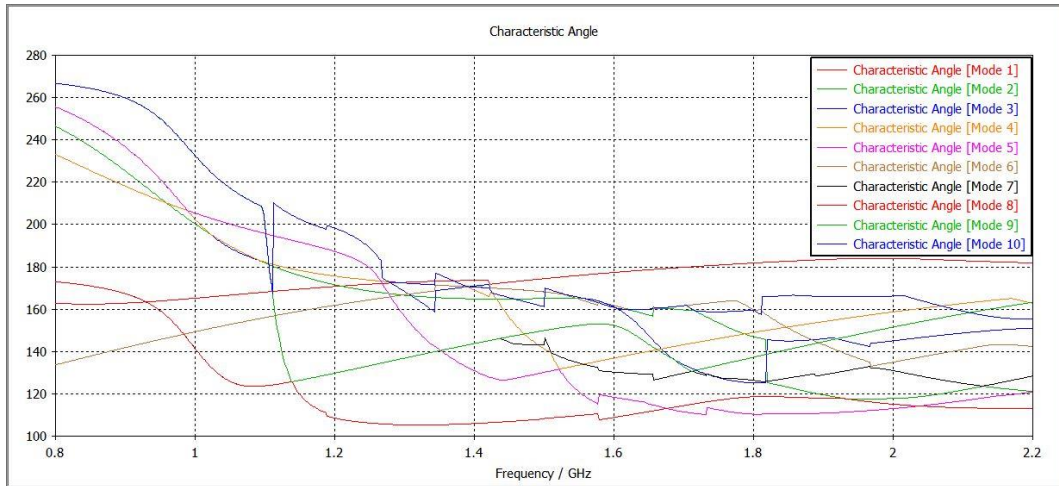


Figure 5.13: Characteristic angles of the complete designed antenna

For illustration, the surface current distribution of the first six modes are listed here in the Tab. 5.4.

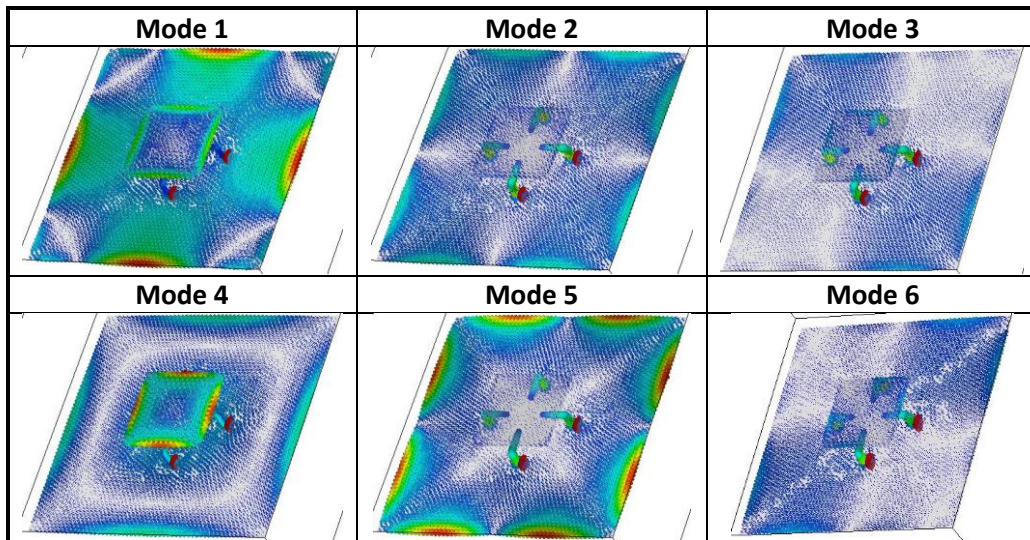


Table 5.4: The surface current distribution for first six modes of the designed antenna

The far-field radiation patterns for Mode 3 and Mode 6 are the following (Tab. 5.5):

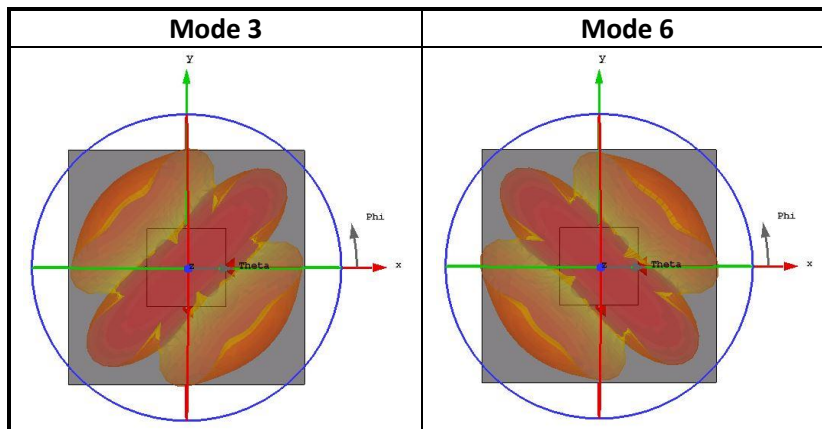


Table 5.5: Far-field radiation patterns of Mode 3 and 6 of the designed antenna

These radiation patterns resemble the radiation patterns of the first two modes of the ground plane itself. However, it can be seen from the surface current distribution diagram that most of the current distribution is concentrated in the vertical part of the L-probes.

The conclusion of the characteristic mode analysis here is the fact, that dominant modes for the radiation are Mode 3 and Mode 6, but the other modes resonating around the center frequency 1.5 GHz contribute to the final cumulative radiation pattern of the designed patch antenna using an L-probe feeding system.

## 5.10 The fabricated sample

The aim of this master thesis is not only the design of an antenna, but also the construction of a working sample. Therefore, the above described patch antenna was constructed and its impedance parameters were measured in the anechoic chamber. The antenna was manufactured fully by hand, so the possibility of construction failures and dimension changes is quite high. Despite the best effort that was made while fabricating the antenna, there was an unintentional change in the dimensions. The differences between the modelled and the constructed antenna are listed in the table. The two dimensions for the parameter  $L_v$  are caused by the fact, that in the end the excited and the parasitic L-probes had different length.

Parameter	Design [mm]	Realization [mm]	$\Delta$ [mm]	$\Delta$ [%]
$H$	27	28.5	+1.5	+5.5
$W$	95	94	-1	-1
$L_h$	32	32	0	0
$L_v$	20	19.5/20.8	-0.5/+0.8	-2.5/+4
$D$	5	5	0	0

Table 5.6: The dimension changes for the fabricated antenna

The production stages and the final fabricated antenna sample is shown in Fig. 5.14.

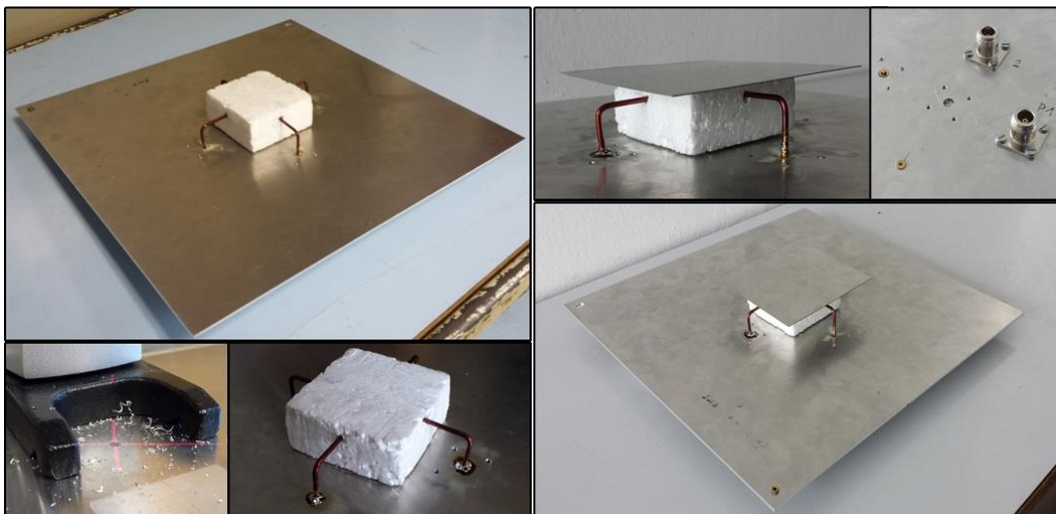


Figure 5.14: Production of the antenna sample

After realization, the antenna sample was measured in the anechoic chamber (Fig. 5.15) to find the input impedance and radiation parameters. The measurement was executed for both ports of the antenna to see the differences between them.

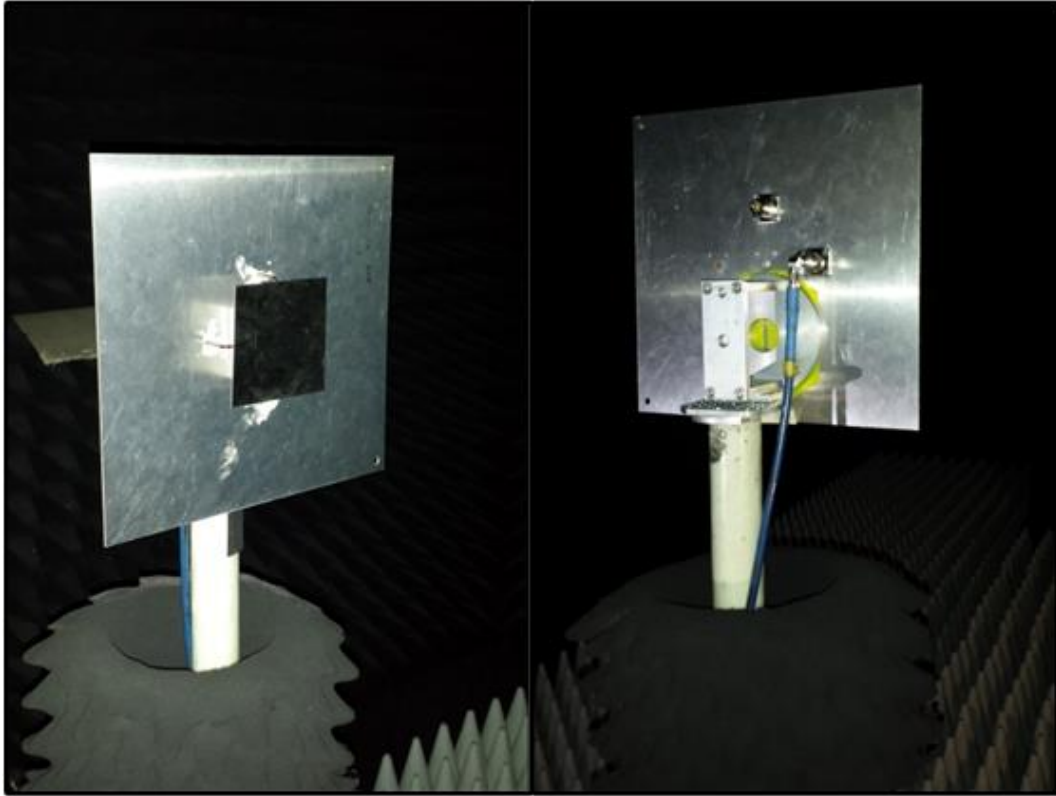


Figure 5.15: The fabricated antenna in the anechoic chamber

After measuring the real dimensions of the fabricated prototype, the whole antenna was resimulated in CST software. This makes the comparison of input impedance parameters with simulation results possible. In the Tab. 5.7, the polar cuts of radiation patterns are listed for the frequency 1.5 GHz. The radiation patterns are measured both in the E- and H-plane. The values are normalized, but unfortunately this plot type in MATLAB does not support negative values. So, practically the maximum value represents 0 dB and the lower values should be understood as negative values.

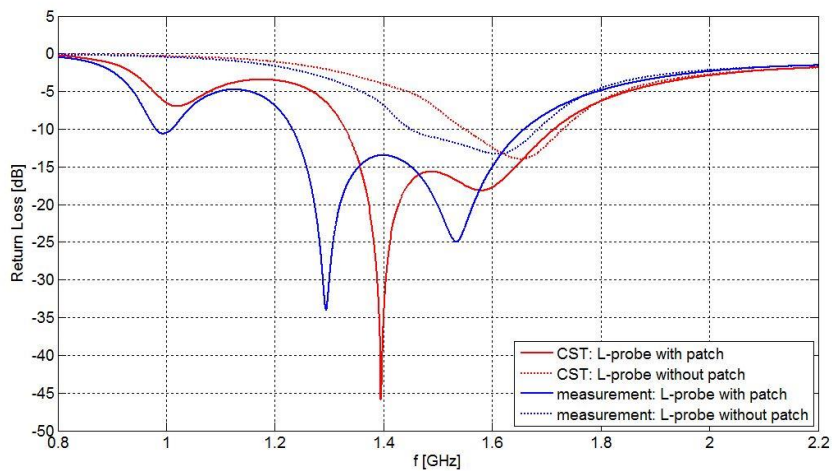


Figure 5.16: The return loss of the fabricated antenna

In Fig. 5.16, the parameter  $S_{11}$  of the antenna is displayed for cases when the structure is with and without patch. It can be observed, that the resonance of the fabricated antenna is shifted by a bit (approximately 500 MHz) to lower frequencies compared with the simulation. The matching is still satisfactory; it is under -10 dB from 1.25 to 1.65 GHz. From Fig. 5.16 can be observed also how the presence of the patch changes the return loss parameter.

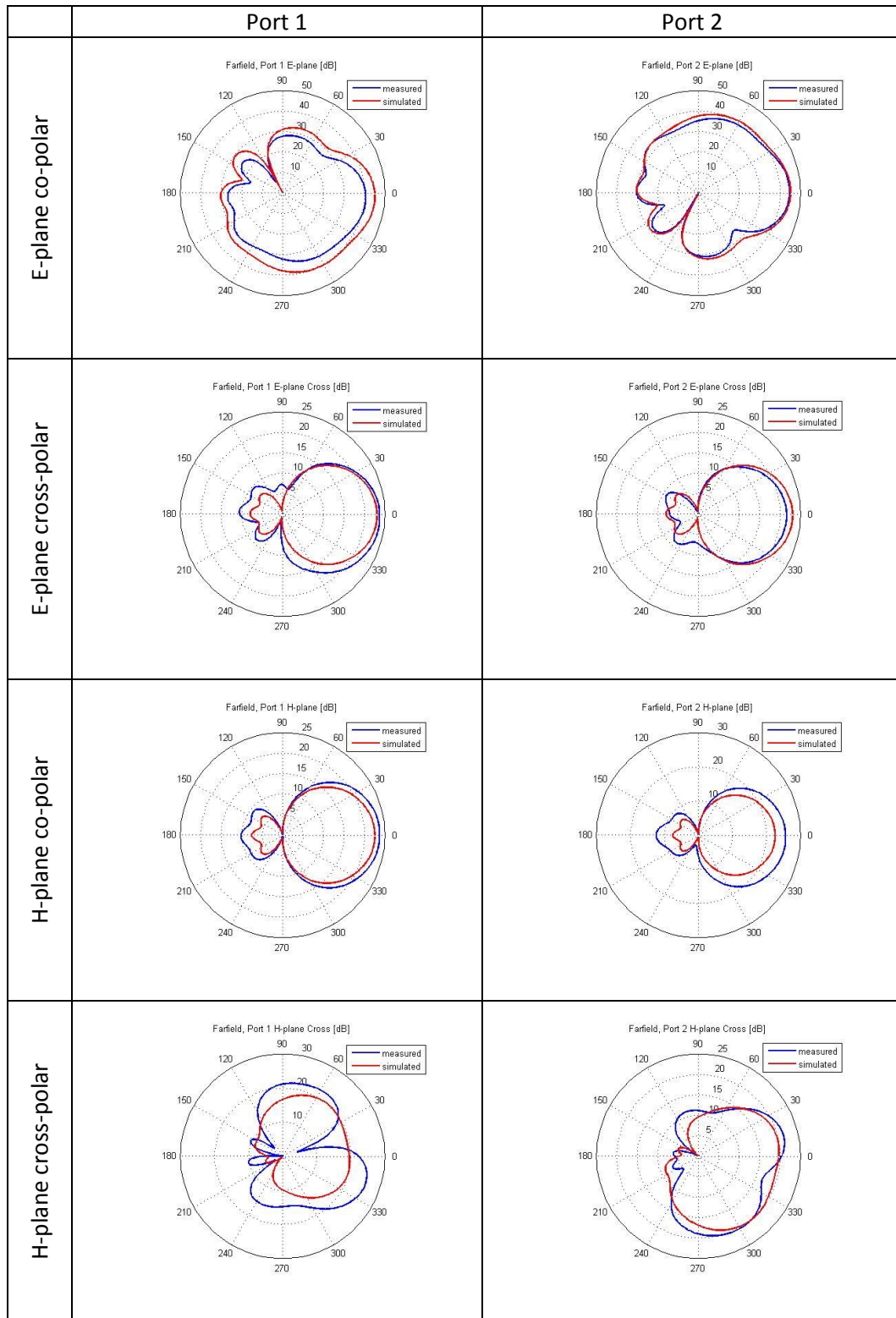


Table 5.7: Comparison of the polar cut radiation patterns from the simulation and measurement

It can be seen from the Tab. 5.7, that the measured and the simulated radiation patterns are mostly similar and comparable to each other. The biggest differences are for the H-plane cross-polarization. The radiation patterns for co-polar polarization in the E-plane are approximately the same for both ports, but they are rotated with respect to each other by 90 degrees and the pattern is mirrored, similarly to the position of the ports in the antenna layout.

In Fig. 5.16, the polarization diagram of the fabricated antenna is depicted. It can be observed, that neither of the polarizations are perfectly aligned, they are shifted in one direction. The polarization pattern of port 1 is shifted more than the same pattern of port 2. This can be explained by the not perfectly symmetrical shape of the crafted patch antenna. The difference between these polarizations is approximately 5 dB in the main direction.

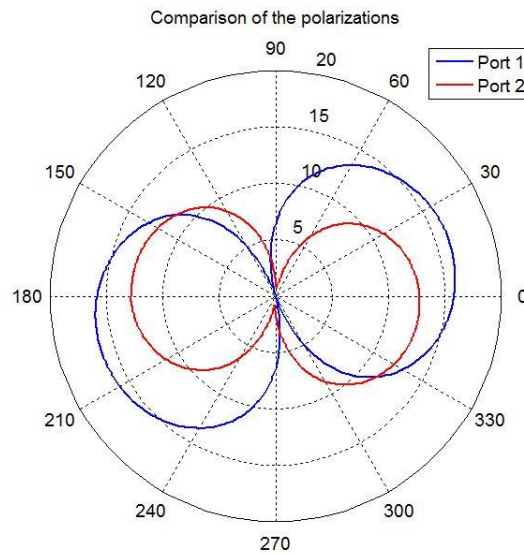


Figure 5.17: The polarization of the fabricated antenna

## 5.11 Summary of the L-probe feeding system

In this chapter of the master thesis, a so called L-probe feeding system was used for excitation of a patch antenna. The biggest advantages of this system are higher achievable impedance bandwidth and high radiation efficiency. At the beginning of the chapter, the behavior of different antenna parameters, such as the length of the vertical and horizontal part of the L-probe, etc., was investigated through a number of parameter sweep simulations. The optimal dimensions for the designed antenna were selected. The designed patch antenna has a square shape, therefore degenerative modes can be successfully excited on the antenna surface. The excitation is provided by two L-probes and two additional parasitic L-probes are present. The final properties of the antenna, like return loss or cross-correlation between the ports, were listed in this section. Furthermore, a characteristic mode analysis was performed in CST. The designed antenna was fabricated and measured in the anechoic chamber. The measured radiation properties were compared with the simulation results. Although, during the production the dimensions of the designed antenna were changed, the fabricated antenna had approximately the same properties as the simulated one. This means, that the L-probe feeding system is fault tolerant within certain limits.



## Chapter 6

# Conclusion

This master thesis dealt with the problematics of polarization diversity antennas. This polarization diversity can be achieved by exciting different modes on the radiator antenna. The thesis is divided into two parts.

The first part of this thesis focuses on the excitation by coupling elements. The aim is to do a research on the existing solutions and concentrate on the use of characteristic modes. With the help of MATLAB scripts the characteristic modes of the square patch antenna were determined and analyzed. These scripts are available from the Department of Electromagnetic Field and consist of several parts which are designed for different purposes in the characteristic mode analysis. Further, the first part of the thesis concentrates on selective excitation of two orthogonal modes with the help of capacitive and inductive coupling elements. As a starting point, the available papers were studied. In the software CST Design Environment, the designed antenna is verified and the radiation patterns are established for each configuration. At the end of the first part, possible matching circuits are described.

It was shown that characteristic modes can be effectively excited by inductive and capacitive coupling elements. Two degenerative modes were excited on a conductive patch surface with dimensions  $10 \times 10$ . With this dimension, the resonant frequency was set to 1.5 GHz. This approximate resonant frequency was achieved in both cases. In this thesis, only one configuration for each coupling element type was investigated and simulated.

Next, the far-field radiation patterns were established. The diagrams made in MATLAB and CST are very similar to each other. The polar cuts of radiation patterns made in CST for each type of coupling elements were compared as well. These comparisons show, that the first two modes of the patch are degenerative and radiate in different polarizations. Also, the suitability of inductive and capacitive coupling elements for exciting the desired modes was proven.

For future work, it would be interesting to examine how the radiation changes in case of different configurations of coupling elements. Properties that could be changed are the sizes of coupling slots and capacitive lines, the location of coupling elements, the number and shape of coupling elements, etc.

The second part of the thesis has a different approach. It focuses on the use of a proximity excitation element, the so called L-probe feeding system. First, the theory and the physical approach of the L-probes was described. Similar to the first half of the master thesis, the aim of this chapter was to design a square patch antenna. The chosen L-probe system was the following: it used two excited L-probes and two parasitic L-probes. The design process was showed in detail. Number of parameter sweep simulations were executed to find out how the antenna parameters react to dimension changes. After that, the optimal lengths of the parameters were selected. The modelled antenna was simulated in CST software. The part of this thesis was also to manufacture a working prototype. This constructed antenna was measured in anechoic chamber. At the end, the properties of the simulated and the measured antenna were discussed and compared. Characteristic mode analysis was performed to find the resonating modes of the designed patch antenna.

An interesting conclusion can be derived from the results. Although the L-probe feeding system has the advantage of wide impedance bandwidth, the use of the parasitic L-probes gives another opportunity to enhance this bandwidth. These parasitic L-probes have their own resonance at lower frequencies than the excited L-probes; with further experiments and proper dimension selection the distance between these two resonant frequencies can be narrowed, consequently the bandwidth broadened.

Another interesting and very useful upgrade would be applying an isolation technique. The antenna now experiences very poor isolation, so in further work this could be the challenge to overcome.

In this thesis, only a squared patch antenna was modelled and used. This simplified the working process because of its symmetry. In further research, it would be interesting to see how the situation changes with different shapes of the patch antenna.

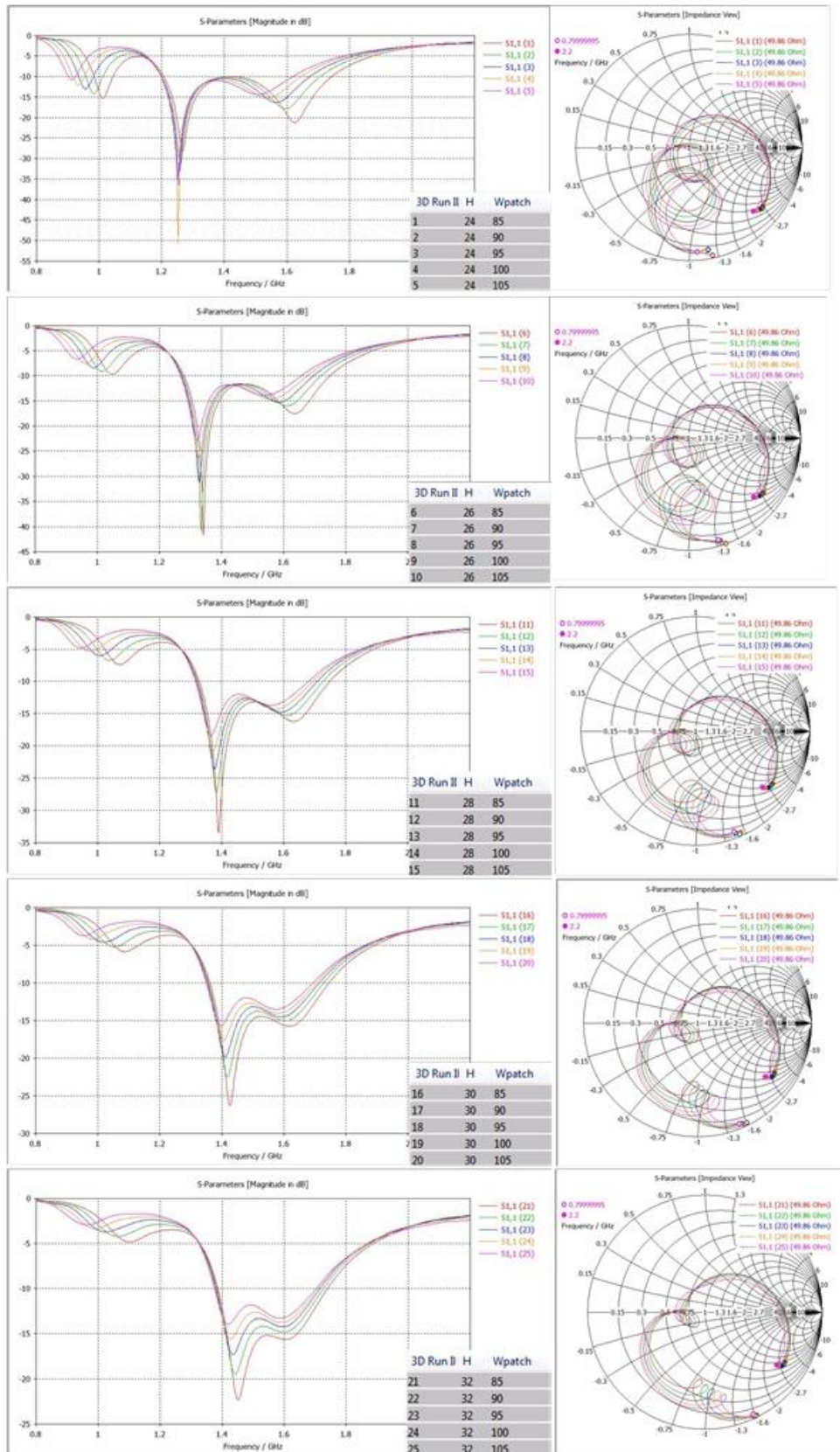
# References

- [1] Morishita H., Kim Y., Fujimoto K.: *Design Concept of Antennas for Small Mobile Terminals and the Future Perspective*, IEEE Antennas and Propagation Magazine, Vol. 44, No. 5, pp. 30-43, October 2002
- [2] Peterson A. F., Ray S. L., Mittra R.: *Computational Methods for Electromagnetics*, New York, IEEE Press/John Wiley, 1997
- [3] Miller E. K., Medgyesi-Mitschang L., Newman E. H. (eds.): *Computational Electromagnetics: Frequency-Domain Method of Moments*, New York, IEEE Press, 1992
- [4] Chong E. K. P., Zak S. H.: *An Introduction to Optimization*, New York, John Wiley & Sons, 2001
- [5] MATLAB, available from www:  
<http://www.mathworks.com/products/matlab/>
- [6] Computer Simulation Technology, available from www:  
<https://www.cst.com/>
- [7] Garbacz R. J., Turpin R. H.: *A Generalized Expansion for Radiated and Scattered Fields*, IEEE Transactions on Antennas and Propagation, AP-19, pp. 348-358, May 1971
- [8] Harrington R. F., Mautz J. R.: *Theory of Characteristic Modes for Conducting Bodies*, IEEE Transactions on Antennas and Propagation, AP-19, 5, pp. 622-628, September 1971
- [9] Harrington R. F., Mautz J. R.: *Computation of Characteristic Modes for Conducting Bodies*, IEEE Transactions on Antennas and Propagation, AP-19, 5, pp. 629-639, September 1971
- [10] Harrington R. F., Mautz J. R.: *Pattern Synthesis for Loaded n-Port Scatterers*, IEEE Transactions on Antennas and Propagation, AP-22, 2, pp. 184-190, March 1974
- [11] Harrington R. F., Mautz J. R.: *Radiation and Scattering from Bodies of Revolution*, Appl. Sci. Res., 20, pp. 405-435, June 1969
- [12] Austin B. A., Murray K. P.: *The Application of Characteristic-Mode Techniques to Vehicle-Mounted NVIS Antennas*, IEEE Transactions on Antennas and Propagation, AP-40, 1, pp. 7-21, February 1998
- [13] Cabedo-Fabrés M., Antonino-Daviu E., Valero-Nogueira A., Bataller M. F.: *The Theory of Characteristic Modes Revisited: A Contribution to the Design of Antennas for Modern Applications*, IEEE Antennas and Propagation Magazine, 49, 5, pp. 52-68, October 2007
- [14] Harrington R. F.: *Field Computation by Moment Methods*, New York, MacMillan, 1968.
- [15] Newman E. H.: *Small Antenna Location Synthesis Using Characteristic Modes*, IEEE Transactions on Antennas and Propagation, AP-21, 6, pp. 868-871, November 1973
- [16] Hamouz P.: *Analýza antén metodou charakteristických modů*, Master Thesis, CTU, 2007

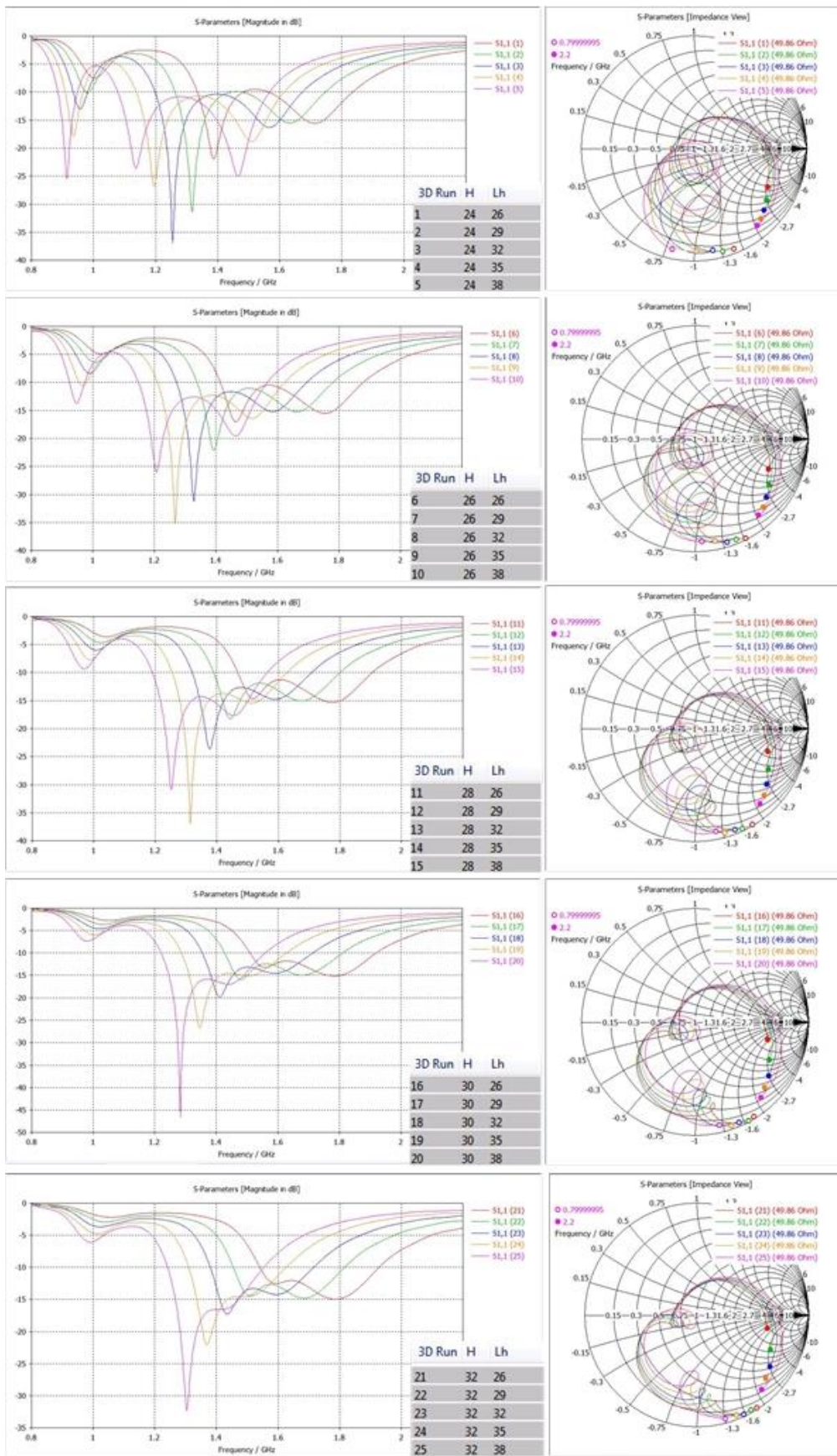
- [17] Neiryneck D., Williams C., Nix A., Beach M.: *Exploiting multiple-input multiple-output in the personal sphere*, IET Microwaves, Antennas and Propagation, vol. 1, Is. 6. pp. 1170-1176, Dec. 2007
- [18] Taruna S., Kaur I.: *Performance Analysis of MIMO for Various Antenna Configurations*, International Conference on Green Computing, Communication and Conservation if Energy, 2013
- [19] Rayi P., Chandra Ch S.: *Performance Evaluation of Channel Capacity in MIMO System*, International Journal of Engineering Research and Application, ISSN 2248-9662, Vol. 1, Issue 4, pp. 1871-1878
- [20] Antonino-Daviu E., Cabedo-Fabres M., Gallo M., Ferrando-Bataller M., Bozzetti M.: *Design of a Multimode MIMO Antenna Using Characteristic Modes*, Antennas and Propagation, EuCAP 2009, 3rd European Conference, pp. 1840-1844, 2009
- [21] Martens R., Safin E., Manteuffel D., *Selective Excitation of Characteristic Modes on Small Terminals*, Antennas and Propagation, EuCap 2011, Proceedings of the 5th European Conference, pp. 2492-2496
- [22] Martens R., Safin E., Manteuffel D.: *Inductive and Capacitive Excitation of the Characteristic Modes on Small Terminals*, Antennas and Propagation Conference, LAPC, Loughborough, 2011
- [23] Wetherell J.: *Impedance Matching Network Designer*, 1997  
<http://home.sandiego.edu/~ekim/e194rfs01/jwmatcher/matcher2.html>
- [24] Le Leivre.com: *LC Impedance matching network designer*  
[http://leleivre.com/rf\\_lcmatch.html](http://leleivre.com/rf_lcmatch.html)
- [25] Hazdra P.: *Planární fraktálové anténní struktury*, Dissertation, CTU, 2009
- [26] Mak C. L., Luk K. M., Kee, K.F., Chow, Y. L.: *Experimental Study of a Microstrip Patch Antenna with an L-Shaped Probe*, IEEE Trans-AP Vol. 48, No. 5, May 2000
- [27] Guo Y., Luk K. W., Lee K-F.: *L-Probe Proximity-Fed Annular Ring Microstrip Antennas*, IEEE, Trans-AP Vol. 49, No. 1, January 2001
- [28] Wong H., Lau K-L., Luk K-M.: *Design of Dual-Polarized L-Probe Patch Antenna Arrays with High Isolation*, IEEE Transactions on Antennas and Propagation, Vol. 52, No. 1, pp. 45-52, January 2004
- [29] Khoo K-W., Guo Y-X., Ong L-C.: *Wideband Dual-Polarized Patch Antenna*, 10<sup>th</sup> IEEE Singapore International Conference on Communication Systems, October 2006
- [30] Hazdra P., Mazánek M., Čermák J.: *Wideband Rectangular Microstrip Patch Antenna Using L-Probe Feeding System*, Radioengineering, Vol. 16, No. 3, September 2007
- [31] Park J., Park J., Choi J., Kim Y-S.: *Ground Slot with Capacitor for High Isolation between MIMO antenna*, 11<sup>th</sup> Mediterranean Microwave Symposium, pp. 197-200, September 2011
- [32] Chen W-S., Lin C-S., Liu H-M.: *MIMO antennas with U-shaped ground and three protrued strips for WLAN applications*, International Workshop on Antenna Technology, pp. 156-159, March 2015

- [33] Isaac A. A., Al-Rizzo H. M., Hammoodi A. I., Khaleel H. R.: *Mutual Coupling Reduction between Two Closely Spaced Inverted-F Antennas*, Radio Science Meeting, July 2015
- [34] Jakes W. C. et al.: *Microwave Mobile Communications*, Hoboken, NJ, USA: Wiley, 1974
- [35] Mikki S. M., Antar Y. M. M.: *On Cross Correlation in Antenna Arrays with Applications to Spatial Diversity and MIMO Systems*, IEEE Transactions on Antennas and Propagation, Vol. 63, No. 4, April 2015
- [36] Blanch S., Romeu J., Corbella I.: *Exact representation of antenna system diversity performance from input parameter description*, Electron. Lett., vol. 39, no. 9, pp. 705-707, May 2003

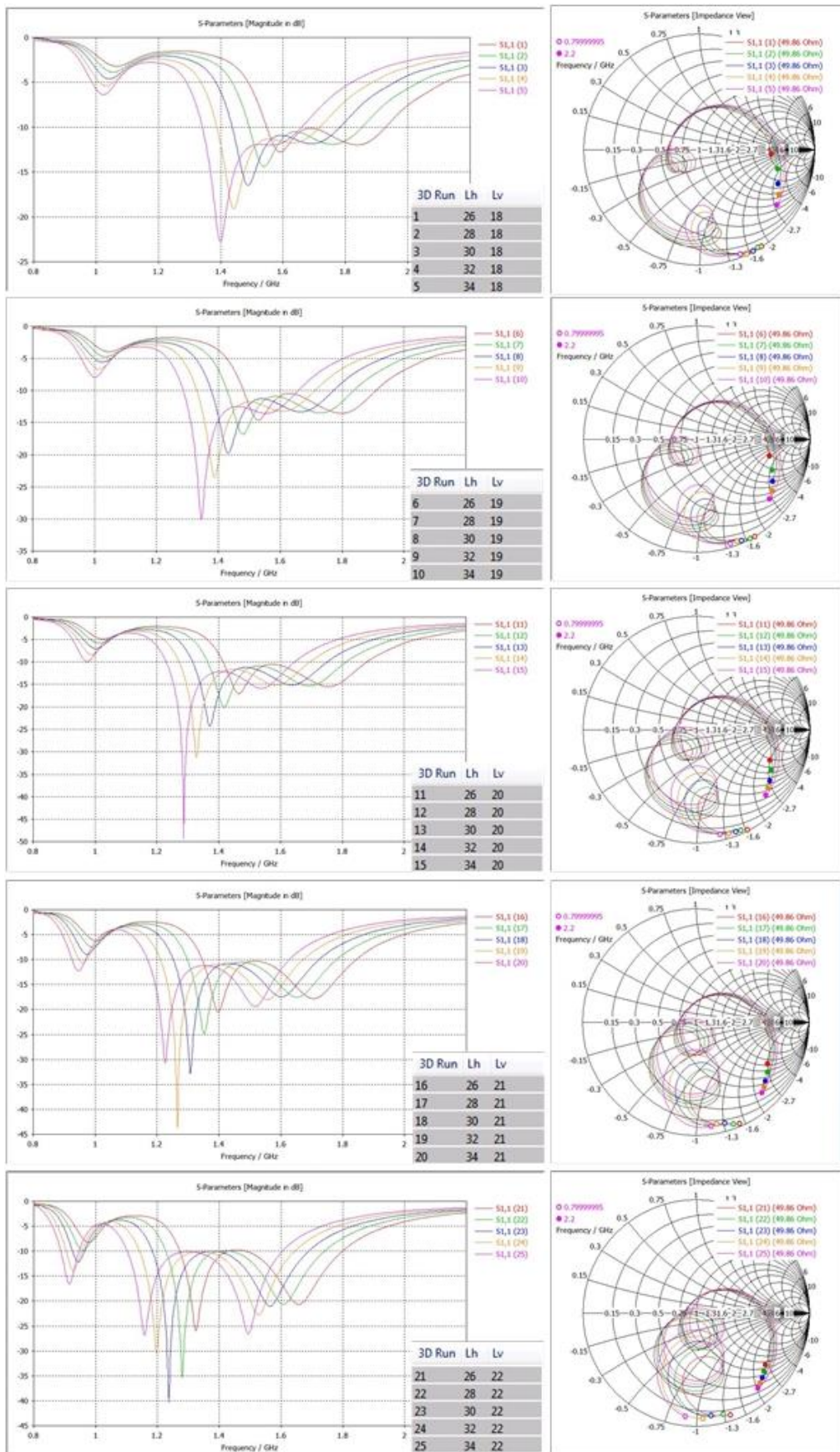
# Appendix



Ap. 1: Parameter sweep simulation,  $H = 24\text{--}32$  mm,  $W = 85\text{--}105$  mm,  $L_v = 20$  mm,  $L_h = 32$  mm



Ap. 2: Parameter sweep simulation,  $H = 24\text{-}32$  mm,  $W = 95$  mm,  $L_v = 20$  mm,  $L_h = 26\text{-}38$  mm



Ap. 3: Parameter sweep simulation,  $H = 26$  mm,  $W = 95$  mm,  $L_v = 18-22$  mm,  $L_h = 26-34$  mm